Published September 17, 2012

Temporal sampling, resetting, and adaptation orchestrate gradient sensing in sperm

Nachiket D. Kashikar,[1,2] Luis Alvarez,[1,2] Reinhard Seifert,[1,2] Ingo Gregor,[2,3] Oliver Jäckle,[1,2] Michael Beyermann,[4] Eberhard Krause,[4] and U. Benjamin Kaupp[1,2]

[1]Department of Molecular Sensory Systems, Center of Advanced European Studies and Research, 53175 Bonn, Germany
[2]Marine Biological Laboratory, Woods Hole, MA 02543
[3]III. Physikalisches Institut, Georg-August Universität, 37077 Göttingen, Germany
[4]Leibniz-Institut für Molekulare Pharmakologie, 13125 Berlin, Germany

Sperm, navigating in a chemical gradient, are exposed to a periodic stream of chemoattractant molecules. The periodic stimulation entrains Ca^{2+} oscillations that control looping steering responses. It is not known how sperm sample chemoattractant molecules during periodic stimulation and adjust their sensitivity. We report that sea urchin sperm sampled molecules for 0.2–0.6 s before a Ca^{2+} response was produced. Additional molecules delivered during a Ca^{2+} response reset the cell by causing a pronounced Ca^{2+} drop that terminated the response; this reset was followed by a new Ca^{2+} rise. After stimulation, sperm adapted their sensitivity following the Weber–Fechner law. Taking into account the single-molecule sensitivity, we estimate that sperm can register a minimal gradient of 0.8 fM/µm and be attracted from as far away as 4.7 mm. Many microorganisms sense stimulus gradients along periodic paths to translate a spatial distribution of the stimulus into a temporal pattern of the cell response. Orchestration of temporal sampling, resetting, and adaptation might control gradient sensing in such organisms as well.

Introduction

Sperm are attracted to the egg by chemical substances, a process called chemotaxis (Eisenbach and Giojalas, 2006; Kaupp et al., 2008). The study of sperm chemotactic signaling is most advanced in marine invertebrates (Ward et al., 1985; Matsumoto et al., 2003; Publicover et al., 2007; Shiba et al., 2008; Guerrero et al., 2010b; Yoshida and Yoshida, 2011; Lishko et al., 2012). In the sea urchin *Arbacia punctulata*, the chemoattractant peptide resact binds to a receptor-type guanylyl cyclase (GC; Shimomura et al., 1986) on the sperm flagellum and rapidly stimulates the synthesis of 3′, 5′-cyclic guanosine monophosphate (cGMP; Kaupp et al., 2003). cGMP opens K^+-selective cyclic nucleotide-gated (CNG; CNGK) channels (Strünker et al., 2006; Galindo et al., 2007; Bönigk et al., 2009). The ensuing transient membrane hyperpolarization opens Ca^{2+} channels (Strünker et al., 2006). The Ca^{2+} influx controls the swimming path (Böhmer et al., 2005; Alvarez et al., 2012). A similar pathway exists in sperm of other sea urchin species and the seastar *Asteria amurensis* (Babcock et al., 1992; Matsumoto et al., 2003; Guerrero et al., 2010a, 2011).

In a shallow recording chamber, sperm trace the chemoattractant gradient along drifting circles (Böhmer et al., 2005). Owing to the looping movement, the stream of molecules impinging on the sperm flagellum is periodically modulated, giving rise to Ca^{2+} oscillations of similar periodicity (Böhmer et al., 2005; Shiba et al., 2008; Guerrero et al., 2010a). Cells or organisms use either spatial or temporal sampling of molecules for chemotactic navigation (Macnab and Koshland, 1972; Dusenbery, 2009; Swaney et al., 2010). Although sperm from various species respond to a chemoattractant surge (Olson et al., 2001; Riffell et al., 2002; Yoshida et al., 2002; Kaupp et al., 2003; Matsumoto et al., 2003; Wood et al., 2005; Gakamsky et al., 2009; Kilic et al., 2009;

N.D. Kashikar and L. Alvarez contributed equally to this paper.

Correspondence to U. Benjamin Kaupp: u.b.kaupp@caesar.de; or Nachiket D. Kashikar: nachiket.kashikar@mrc-lmb.cam.ac.uk

N.D. Kashikar's present address is Neurobiology Division, Medical Research Council Laboratory of Molecular Biology, CB2 0QH Cambridge, England, UK.

Abbreviations used in this paper: ASW, artificial sea water; CCD, charge-coupled device; cGMP, cyclic guanosine monophosphate; CNG, cyclic nucleotide gated; GC, guanylyl cyclase; i.d., inner diameter; mPIC, mammalian tissue protease inhibitor cocktail; NCKX, Na^+/Ca^{2+}-K^+ exchanger; TFA, trifluoroacetic acid; V_m, membrane voltage.

Supplemental Material can be found at:
http://jcb.rupress.org/content/suppl/2012/09/13/jcb.201204024.DC1.html

The Rockefeller University Press $30.00
J. Cell Biol. Vol. 198 No. 6 1075–1091
www.jcb.org/cgi/doi/10.1083/jcb.201204024

Published September 17, 2012

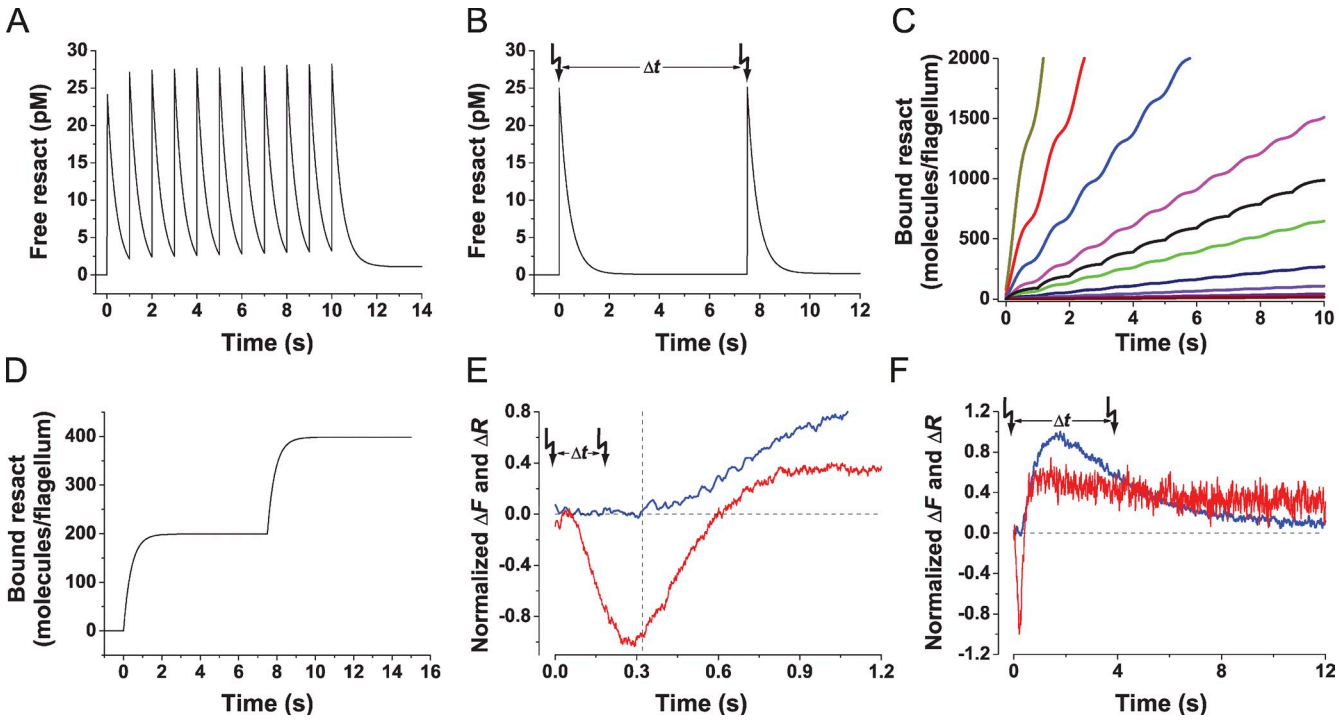

Figure 1. **Illustration of the experimental rationale.** (A) Simulated stimulus function for a sperm exposed to repetitive pulses of resact: a time interval Δt = 1 s each. Stimulus function was calculated using Eq. 3. (B) Stimulus function for paired resact stimuli with longer Δt. (C and D) Time course of bound resact molecules per flagellum. (C, black line) Repetitive pulses of resact. (C, colored lines) Sperm, swimming on a circular path in a chemoattractant gradient, at different distances from the egg (in millimeter): 2.1, dark yellow; 2.2, red; 2.3, blue; 2.4, magenta; 2.5, green; 2.6, navy; 2.7, violet; 2.8, purple; 2.9, wine. (D) Two resact pulses at long Δt. (E) A second stimulus delivered during the latency (interrupted lines) of the Ca^{2+} signal probed temporal sampling. Latency of the Ca^{2+} signal (blue) matches the time to peak of the hyperpolarization V_m signal (red). (F) Complete time course of a typical V_m (red) and a corresponding Ca^{2+} signal (blue). In paired stimulus experiments, the second stimulus was delivered at different phases of the Ca^{2+} and V_m signals. Arrows indicate time of flashes.

Morita et al., 2009; Guerrero et al., 2010a; Burnett et al., 2011), it is not known which sampling strategy is used by sperm for gradient sensing. Furthermore, in the natural habitat, sperm are exposed to both continuous gradients and discontinuous chemoattractant fields (plumes) separated by voids (Riffell and Zimmer, 2007; Zimmer and Riffell, 2011). It is not known how sperm respond to successive steplike stimulation by plumes. How do sperm process spatiotemporal patterns of chemoattractant as complex as plumes in a turbulent environment or a smooth chemoattractant distribution in the quiet sea? *A. punctulata* sperm are exquisitely sensitive: they respond to binding of a single resact molecule (Kaupp et al., 2003; Strünker et al., 2006; Bönigk et al., 2009). However, during their sojourn in a gradient, sperm get exposed to an ever increasing chemoattractant concentration spanning several orders of magnitude (Kaupp et al., 2003; Strünker et al., 2006). How do sperm adjust their sensitivity to escape signal saturation?

Finally, although sperm chemotaxis has been studied for a century (Lillie, 1912, 1913), several fundamental questions remain unanswered: What is the effective geometrical range over which the chemoattractant gradient disperses with time? And, how far away from the egg can sperm be attracted?

To study these questions, we used rapid kinetic techniques to follow the changes in membrane voltage (V_m) and intracellular Ca^{2+} concentration $[Ca^{2+}]_i$. We used flash photolysis of caged analogues of resact and cGMP (Hagen et al., 2001, 2002, 2003; Kaupp et al., 2003) to implement a paired stimulus paradigm that emulates periodic stimulation both in continuous gradients and discontinuous concentration fields. Moreover, we measured the amount of resact released from an egg and simulated a gradient pattern formed by diffusion.

Results

Experimental rationale

We studied signaling in sperm by a combination of the stopped-flow method and flash photolysis. In brief, a sperm suspension in a microcuvette was rapidly stimulated with resact. After various time intervals (Δt), an additional resact stimulus was delivered via flash photolysis of caged resact (Kaupp et al., 2003). We modeled the kinetics of the binding reaction for different Δt to derive the stimulus function, i.e., the time course of bound and free resact (Eq. 3 in Materials and methods section; Fig. 1, A and B). After exposing sperm to resact either by mixing or photorelease, the free concentration increased in a steplike fashion and then decreased because resact binds to receptors on the sperm flagellum. The step increase is set either by the mixing time (1 ms) or the photorelease, and the decrease is shaped by the kinetics of equilibration between free and bound resact. For these experiments, the receptor concentration was in vast excess; therefore, most resact molecules became bound. Repetitive pulses of resact mimic the periodic stimulation of sperm that swim on drifting circles in a chemical gradient (Fig. 1, A and C), whereas paired stimuli with long Δt mimic the

Published September 17, 2012

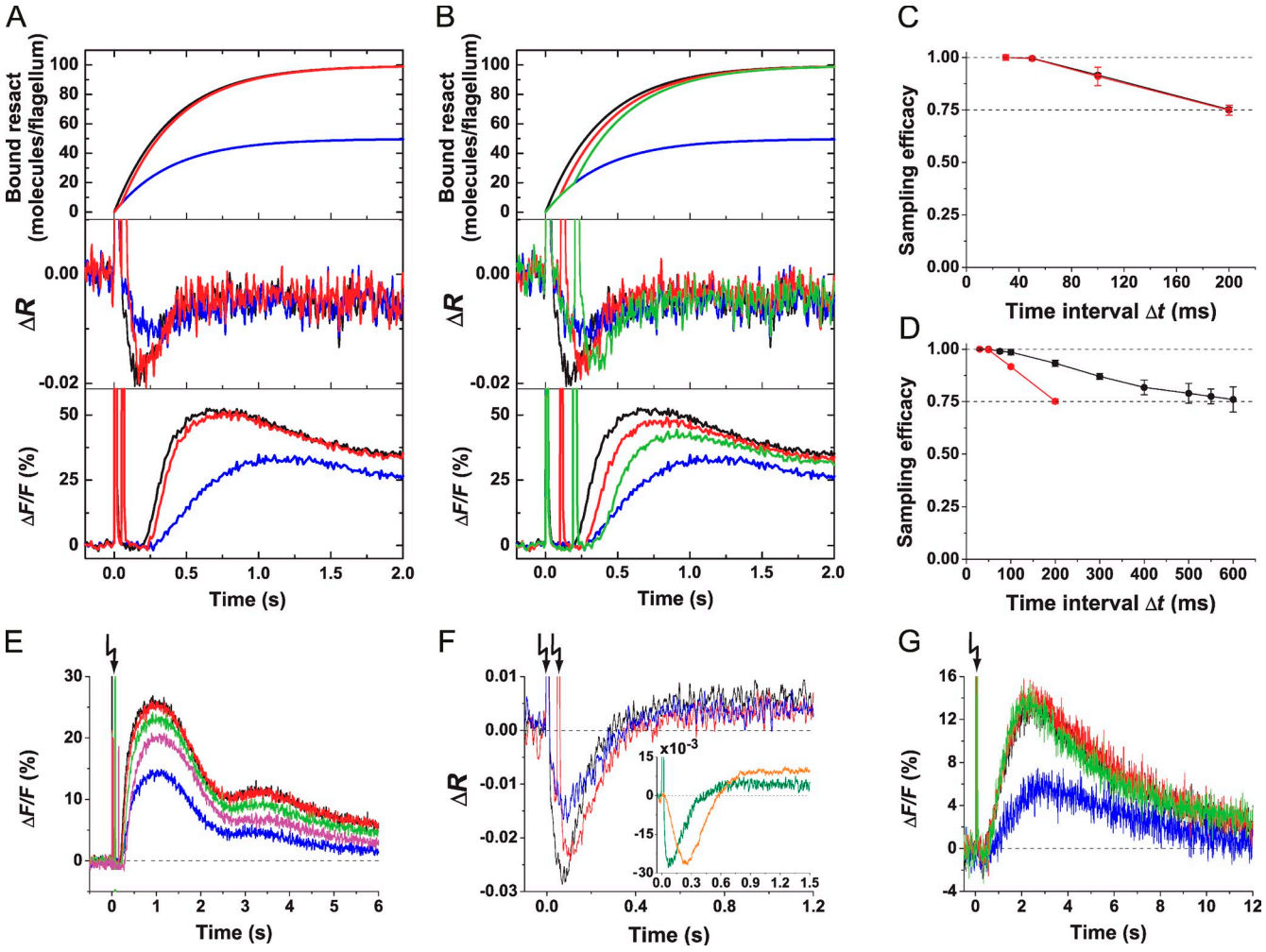

Figure 2. **Sperm temporally sample chemoattractant molecules.** (A and B) Identical paired stimuli of 12.5 pM resact were delivered by photolysis of 100 nM caged resact; stimulus functions (top), V_m signals (middle), and Ca^{2+} signals (bottom) are shown. Flashes in A: single 50% (blue), single 100% (black), and paired 50% with Δt = 50 ms (red). Flashes in B: single 50% (blue), single 100% (black), and paired 50% with Δt = 100 ms (red) or 200 ms (green). (C) Decrease of sampling efficacy of V_m (red) and Ca^{2+} (black) signals with increasing Δt. Three experiments as shown in A and B were analyzed. The V_m and Ca^{2+} signals evoked by a full intensity flash were normalized to 0 (baseline) and 1 (peak amplitude). The signal amplitudes evoked by paired half-intensity flashes were scaled to these two values. (D) Sampling efficacy depends on stimulus strength. The low stimulus strength regimen was achieved using 10 nM caged resact and flashes of 25 and 50% (black; n = 4). The high stimulus strength regimen was achieved using 100 nM caged resact and flashes of 50 and 100% (red; n = 3). (E) Sperm temporally sample changes in cGMP concentration. Ca^{2+} signals were evoked by photolysis of caged cGMP. Flashes: single 10% (blue), single 20% (black), and two 10% with a Δt of 30 ms (red), 75 ms (green), or 150 ms (magenta). (F) V_m signals evoked by paired stimuli of cGMP. Flashes: single 8% (blue), single 16% (black), and two 8% with Δt = 50 ms (red). (Inset) V_m signals of identical amplitude evoked by cGMP (green) and resact (orange). (G) Sperm count single resact molecules. Ca^{2+} signals were evoked by releasing ~625 fM resact (blue), single full intensity flash (1.25 pM; black), and two half-intensity flashes (625 fM each) with Δt = 30 ms (red) or 75 ms (green). Error bars show SDs. Arrows indicate time of flashes.

steplike stimulation while swimming in plumes of chemoattractant (Fig. 1, B and D). Specifically, the second stimulus was along different phases of V_m or Ca^{2+} signals (Fig. 1, E and F): (a) during the latency of a Ca^{2+} signal to probe temporal sampling of resact molecules and cellular integration of binding events (Fig. 1 E); (b) during an emerging Ca^{2+} signal to probe how stimuli are discerned (Fig. 1 F); and (c) during or after signal recovery to probe the adjustment of the cell's sensitivity to ambient chemoattractant concentration.

Sperm temporally sample chemoattractant molecules

We studied temporal sampling of contiguous binding events by measuring the V_m signal produced by paired stimuli that were delivered by flash photolysis of caged resact. The second stimulus was delivered during the hyperpolarizing phase of the V_m signal, i.e., during the latency of the Ca^{2+} signal (Fig. 1 D). The first flash with a relative strength of 50% released ~12.5 pM resact from caged resact (for experimental details see Fig. S1). A second 50% flash was delivered with a Δt between 30 and 200 ms. We plotted the number of bound resact molecules for different Δt and for one 100% versus two 50% flashes (Fig. 2, A and B, top). For short Δt, the time course of bound resact after two 50% flashes is similar to that of a single 100% flash. For longer Δt, the time course of bound resact for two flashes versus one flash became distinct. As a consequence, for $\Delta t \leq 50$ ms, the respective V_m signals were almost identical (Fig. 2 A, middle), whereas for $\Delta t \geq 50$ ms, the summed V_m signals peaked later and

Published September 17, 2012

became progressively smaller (Fig. 2 B, middle). The longer time to peak can be explained by the prolonged cGMP synthesis, which opens additional CNGK channels and, thereby, extends the rising phase of the hyperpolarization. Thus, sperm discriminate pulses for long, but not short, Δt.

We quantified stimulus integration by the ratio of V_m amplitude (ΔV_m) evoked by two 50% flashes/one 100% flash. We refer to this ratio as "sampling efficacy." Sampling efficacy is unity if ΔV_m evoked by two 50% flashes is equal to that evoked by a single 100% flash. Sampling efficacy was unity for $\Delta t \leq 50$ ms and declined for longer Δt (Fig. 2 C). Ca^{2+} signals were studied by the same protocol (Fig. 2, A and B, bottom). For time intervals $\Delta t \leq 50$ ms, Ca^{2+} signals evoked by one 100% flash or two 50% flashes were almost identical in amplitude, slope, and waveform (Fig. 2, A and B, bottom; and Fig. S2 A for a complete time course). With increasing Δt, Ca^{2+} signals displayed a longer latency caused by the longer time to peak of V_m signals produced by a pair of flashes (Fig. 2 A, middle). In a similar vein, the sampling efficacy of Ca^{2+} signals declined with increasing Δt (Fig. 2, B [bottom] and C; and Fig. S2 B for a complete time course). When stimuli of different strength were used, the decline was more pronounced for strong compared with weak stimuli (Fig. 2 D). The Ca^{2+} signal, which triggers the physiological response, begins to rise 0.2–0.6 s after stimulation. Because resact binding still takes place at this time (Fig. 1), a fraction of molecules arrives after the onset of the Ca^{2+} signal; these latecomers are not integrated into the sum response. This effect might account for the decrease of sampling efficacy at long Δt.

We also studied sampling efficacy with paired cGMP stimuli delivered by photolysis of caged cGMP (Fig. 2 E): for short Δt, summation of Ca^{2+} signals was perfect. Thus, sperm integrate for some time the changes in intracellular cGMP concentration. However, using caged cGMP, V_m signals do not sum perfectly: the amplitude of V_m signals evoked by two flashes ($\Delta t = 50$ ms) was smaller than that evoked by a single flash of twice the energy (Fig. 2 F). The reason might be that the V_m signals evoked by cGMP rose extremely fast compared with resact-evoked signals (Fig. 2 F, inset). Probably, counterbalancing conductances are quickly activated and prevent perfect summation.

In summary, sperm collect molecules for some time before evoking a Ca^{2+} response; we refer to this time window as the sampling time. Multiple stimuli delivered during the sampling time are integrated to produce a single V_m and Ca^{2+} signal. Sampling efficacy is perfect for short sampling times and declines for longer times.

Sperm can count single molecules

For low resact concentrations, prevailing at the foot of a gradient, only few molecules hit the flagellum. We examined how individual molecules that arrive at the flagellum are processed. Caged resact concentration and flash intensity were adjusted such that ~625 fM resact was released, which is about one bound molecule per cell (Kaupp et al., 2003) (Fig. 2 G). The Ca^{2+} signals, evoked by two resact molecules either delivered successively ($\Delta t \leq 75$ ms) or at once, were identical (Fig. 2 G). Thus, in the single-molecule regime, not only do sperm detect but also faithfully count single resact molecules to produce a sum response.

A second stimulus during a Ca^{2+} response resets the cell

The dynamics rather than the absolute $[Ca^{2+}]_i$ controls the swimming path (Alvarez et al., 2012). Therefore, we studied how a second stimulus affects an ongoing Ca^{2+} signal. When delivered at the peak of a Ca^{2+} signal ($\Delta t = 1$ s), both cGMP and resact first caused a rapid and profound Ca^{2+} decrease followed by a Ca^{2+} rise (Fig. 3 A and Fig. S2 C). This finding confirms previous observations on sperm from another sea urchin *Strongylocentrotus purpuratus* (Nishigaki et al., 2004), although the Ca^{2+} drop is much more profound in *A. punctulata* (Fig. 3 A and Fig. S2 E). The first and second Ca^{2+} signals are almost identical in waveform as illustrated by shifting the t axis by the flash interval $-\Delta t$ (Fig. 3 A, inset).

In *S. purpuratus* sperm, two different mechanisms—Na^+/Ca^{2+}-K^+ exchanger (NCKX; Su and Vacquier, 2002) and Ca^{2+}-ATPase activity (Gunaratne and Vacquier, 2006)—contribute to Ca^{2+} extrusion. We reasoned that similar mechanisms might exist in *A. punctulata*. By mass spectrometry, we identified peptides of both proteins in flagella of *S. purpuratus*, yet only peptides for NCKX from *A. punctulata* flagella (Tables S1, S2, and S3). To provide evidence for the involvement of NCKX in the Ca^{2+} drop in *A. punctulata* sperm, we used a well-known NCKX blocker, KB-R7943 mesylate. However, the blocker displayed strong nonspecific effects on Ca^{2+} signals (Fig. S3) and completely inhibited sperm motility (Su and Vacquier, 2002), preventing further use. Therefore, we used the voltage dependence of NCKX to study the Ca^{2+} drop mechanism. Each resact stimulus produced a transient hyperpolarization (Fig. 3 B and Fig. S2 D). The Ca^{2+} drop followed the hyperpolarization without any latency (Fig. 3 B, inset), most likely because activated Ca_v channels close (Perez-Reyes, 2003), and NCKX activity is enhanced (Cervetto et al., 1989; Lagnado and McNaughton, 1990; Blaustein and Lederer, 1999; Su and Vacquier, 2002). The hyperpolarization and also the depth and slope of the Ca^{2+} drop were graded with flash intensity (Fig. 3, C and D, respectively). The voltage dependence of Ca_v channels is steep (Perez-Reyes, 2003), whereas that of NCKX is shallow (Lagnado et al., 1988). We find a shallow, almost linear relation between hyperpolarization and slope of the Ca^{2+} drop (Fig. 3 E), arguing that NCKX activity is mainly responsible for the Ca^{2+} drop.

The activity of NCKX depends on the level of prevailing $[Ca^{2+}]_i$. To investigate the Ca^{2+} dependence, identical flashes were delivered at different Δt along an unfolding Ca^{2+} signal (Fig. 3 F). The lower $[Ca^{2+}]_i$, the smaller both the Ca^{2+} drop (Fig. 3, G and H) and the rate of the Ca^{2+} drop (Fig. 3 I), consistent with the idea that NCKX is involved in Ca^{2+} extrusion. Of note, we cannot exclude that other molecules, such as Ca^{2+}-ATPase activity, also participate.

In conclusion, a stimulus during an ongoing Ca^{2+} response terminates Ca^{2+} signaling, rapidly lowers $[Ca^{2+}]_i$, and then initiates a new Ca^{2+} rise. We define this process as a reset mechanism.

Ca^{2+} signals can be reset with a frequency of ≥1 Hz

In a chemical gradient, sperm are periodically stimulated with the angular frequency of circular swimming of ~1 Hz

Published September 17, 2012

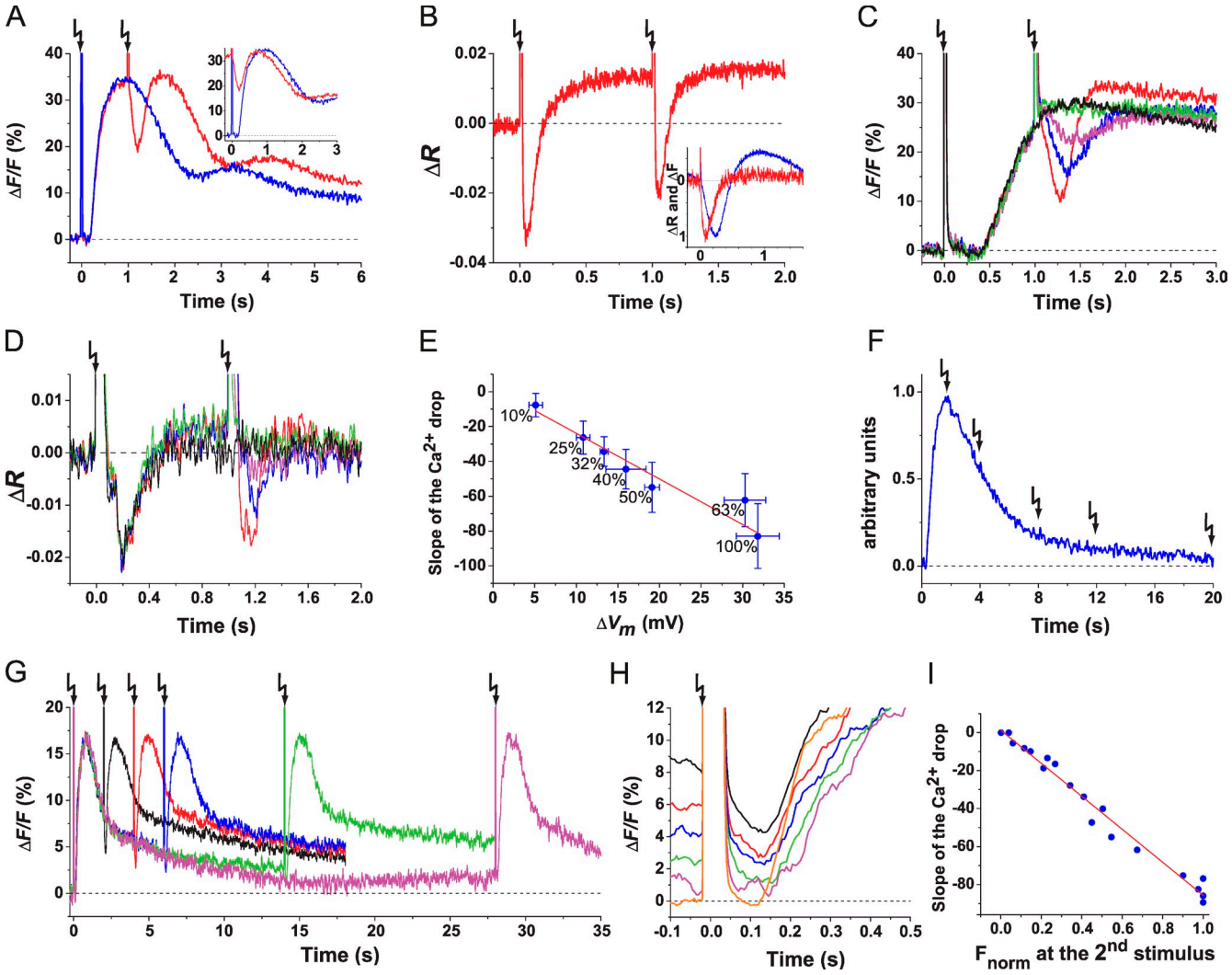

Figure 3. **A second stimulus produces a Ca^{2+} drop followed by a new Ca^{2+} rise.** (A) Ca^{2+} signals were evoked by cGMP. Single 25% flash (blue) and two identical 25% flashes (red; Δt = 1 s) are shown. (inset) The second Ca^{2+} signal was shifted by $-\Delta t$ to the left and superposed on the first Ca^{2+} signal. (B) V_m signals evoked by paired cGMP stimuli (Δt = 1 s). (inset) Kinetics of the Ca^{2+} drop (blue) and the hyperpolarization (red) evoked by the second stimulus. Downward peaks of the Ca^{2+} drop and the hyperpolarization were normalized. (C and D) Ca^{2+} (C) and V_m (D) signals. Paired stimuli (caged resact of 100 nM) were delivered. Intensity of the first flash was kept constant at 50%, and intensity of the second flash (Δt = 1 s) was varied (in percentage): 10 (green), 25 (magenta), 50 (blue), and 100 (red). For comparison, a 50% flash signal without second flash is shown (black). (E) Relationship between ΔV_m after the second flash and slope of the Ca^{2+} drop. The plot was constructed from experiments as in C and D (V_m signals, n = 4; Ca^{2+} signals, n = 3). Absolute values in millivolts for ΔV_m were obtained from ΔR signals as previously described in Strünker et al. (2006). A linear regression was fitted through data points. Numbers near data points indicate the intensity of the second flash. Error bars show SDs. (F) Scheme of the delivery of a second stimulus at different Δt along a Ca^{2+} signal. (G) Paired cGMP flashes (10% each) were delivered with Δt (in seconds) of 2 (black), 4 (red), 6 (blue), 14 (green), and 28 (magenta). (H) Comparison of Ca^{2+} drops evoked by the second flash at various Δt as in G. The second flashes were aligned to t = 0 by shifting the x axis to the left by the respective $-\Delta t$. The fluorescence before t = 0 shows the $[Ca^{2+}]_i$ at the time of the second flash. The Ca^{2+} signal evoked by the first flash is shown in orange. (I) Ca^{2+} drop amplitude (ΔF_{drop}) versus Ca^{2+} level (F_{norm}) at the time of the second flash (blue symbols, n = 21). To compare across experiments, Ca^{2+} signals were normalized to 0 (baseline Ca^{2+} signal) and 1 (Ca^{2+} signal amplitude after the first flash). A linear regression was fitted (R^2 = 0.98). Arrows indicate time of flashes.

(Böhmer et al., 2005). We emulated this periodic stimulation by challenging sperm with a train of identical flashes (1 Hz) each delivering a pulse of cGMP. The repetitive stimulation produced a train of Ca^{2+} signals (Fig. 4 A) triggered by a train of hyperpolarizing pulses (Fig. 4 B). Each flash initiated a Ca^{2+} drop followed by a Ca^{2+} rise. The pattern of Ca^{2+} results from the superposition of two opposing processes—termination of an ongoing Ca^{2+} signal and generation of a new one. Thus, signals appear as Ca^{2+} oscillations superposed on an elevated Ca^{2+} level (Fig. 4 A). During a train of stimuli, Ca^{2+} signals rose progressively slower, indicating that some kind of adaptation kicked in (Fig. 4 C, inset). The underlying V_m signals might offer an explanation: although time course and ΔV_m of successive V_m signals were identical (Fig. 4 D), a steady increase of the V_m baseline occurred with increasing flash number (Fig. 4 B), which possibly altered the kinetics of Ca^{2+} channel activation. In summary, sperm can produce V_m and Ca^{2+} responses with ≥1 Hz, the frequency of periodic steering responses in a gradient.

The Ca^{2+} drop affects path curvature

To study the functional significance of the Ca^{2+} drop, we simultaneously recorded the changes in $[Ca^{2+}]_i$ and the swimming

Published September 17, 2012

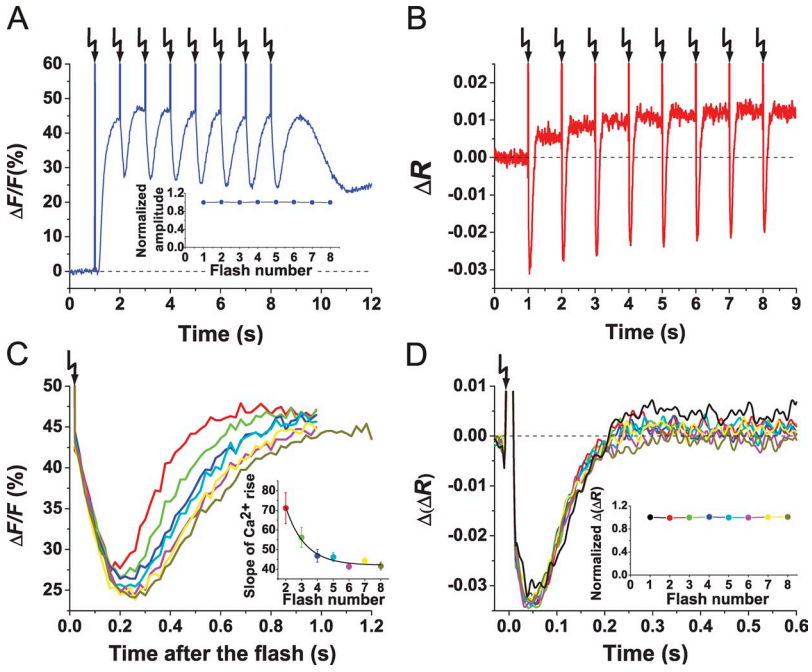

Figure 4. **Sperm encode periodic stimuli.** (A and B) Ca^{2+} (A) and V_m (B) signals upon repetitive stimuli of cGMP (25% flash; Δt = 1 s). (A, inset) Plot of peak amplitudes of Ca^{2+} rises after each flash. The Ca^{2+} signal amplitude after the first flash was taken as 1, and subsequent amplitudes were normalized (n = 6). (C) Superposition of Ca^{2+} drops as in A. Each trace represents the flash depicted in A. Flash number: second (red), third (green), fourth (blue), fifth (cyan), sixth (magenta), seventh (yellow), and eighth (dark yellow). Ca^{2+} drops were aligned to the time of the respective flash. (inset) Slope of Ca^{2+} rise after the drop after each flash (n = 6). Error bars are SDs. (D) Superposition of V_m signals as in B. Flash number: first (cyan), second (black), third (red), fourth (blue), fifth (green), sixth (magenta), seventh (dark yellow), and eighth (navy). For superposition, signals were aligned to the time of the respective flash. (inset) Plot of V_m amplitude ($\Delta(\Delta R)$) after each flash. To compare across different trials (n = 5), ΔV_m after the first flash was taken as 1, and subsequent amplitudes were normalized. Arrows indicate time of flashes.

path of single cells. Although the Ca^{2+} waveform varied from cell to cell, the basic features of the population Ca^{2+} signals were conserved (Fig. 5 A and Video 1): the first flash, after a short latency, evoked a Ca^{2+} rise, whereas the second flash, delivered at the peak of a Ca^{2+} signal, produced a Ca^{2+} drop followed by a new Ca^{2+} rise (Fig. 5 A).

We compared Ca^{2+} signals and swimming paths of sperm that received either one (Fig. 5 B) or two stimuli (Fig. 5 C). Sperm that received a second stimulus responded to the Ca^{2+} drop with an abrupt change in the swimming path: the curvature $\kappa(t)$ decreased and can even reverse sign (Fig. 5 C and Video 1; Alvarez et al., 2012). Apparently, the Ca^{2+} drop leads to an extension of the straighter swimming period. During the subsequent Ca^{2+} rise, $\kappa(t)$ increased again, resulting in a new turn (Fig. 5 C).

The swimming path can be numerically reconstructed from Ca^{2+} signals and the swimming speed ($s(t)$; Alvarez et al., 2012). Compared with single sperm, Ca^{2+} signals recorded from a sperm population exhibited a better signal-to-noise ratio (S/N) and were highly uniform. Hence, we calculated the swimming

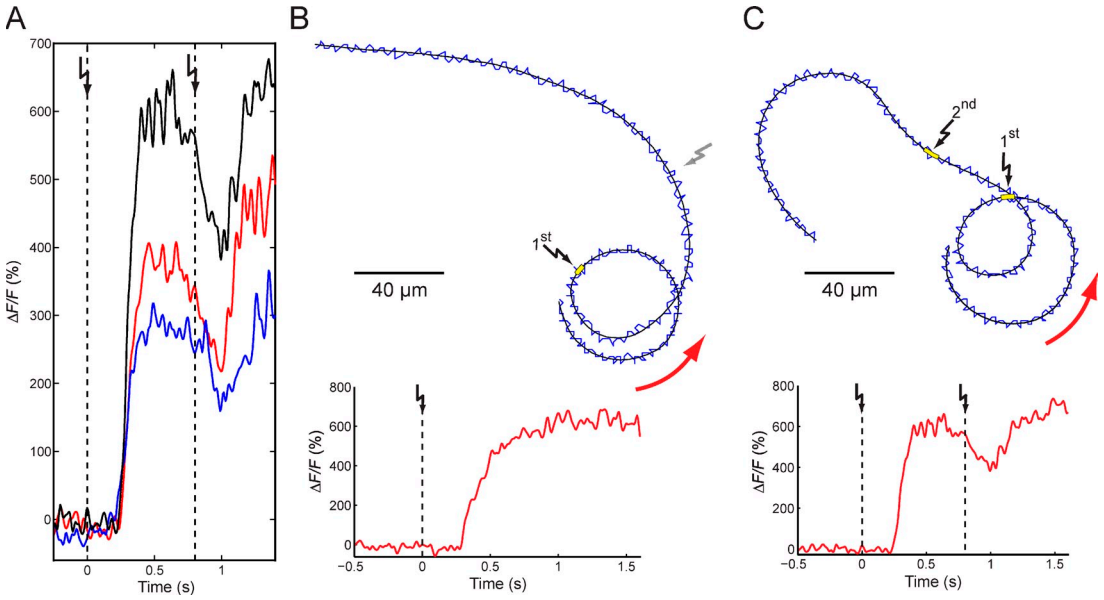

Figure 5. **Ca^{2+} drop in single cells.** (A) Ca^{2+} signals from three different cells (depicted in three different colors) evoked by paired cGMP flashes (dashed lines; Δt = 800 ms). (B and C) Representative swimming paths and corresponding Ca^{2+} signals from single cells after a single flash (B, yellow box and black flashes) or two flashes (Δt = 800 ms; C, yellow boxes and black flashes). The head (blue traces) wiggles around the average path (black trace). Swimming direction is shown by red arrows. After the second flash (C), the swimming path transiently bent in a clockwise direction, whereas the control cell swam undeviated (B, gray flash).

Published September 17, 2012

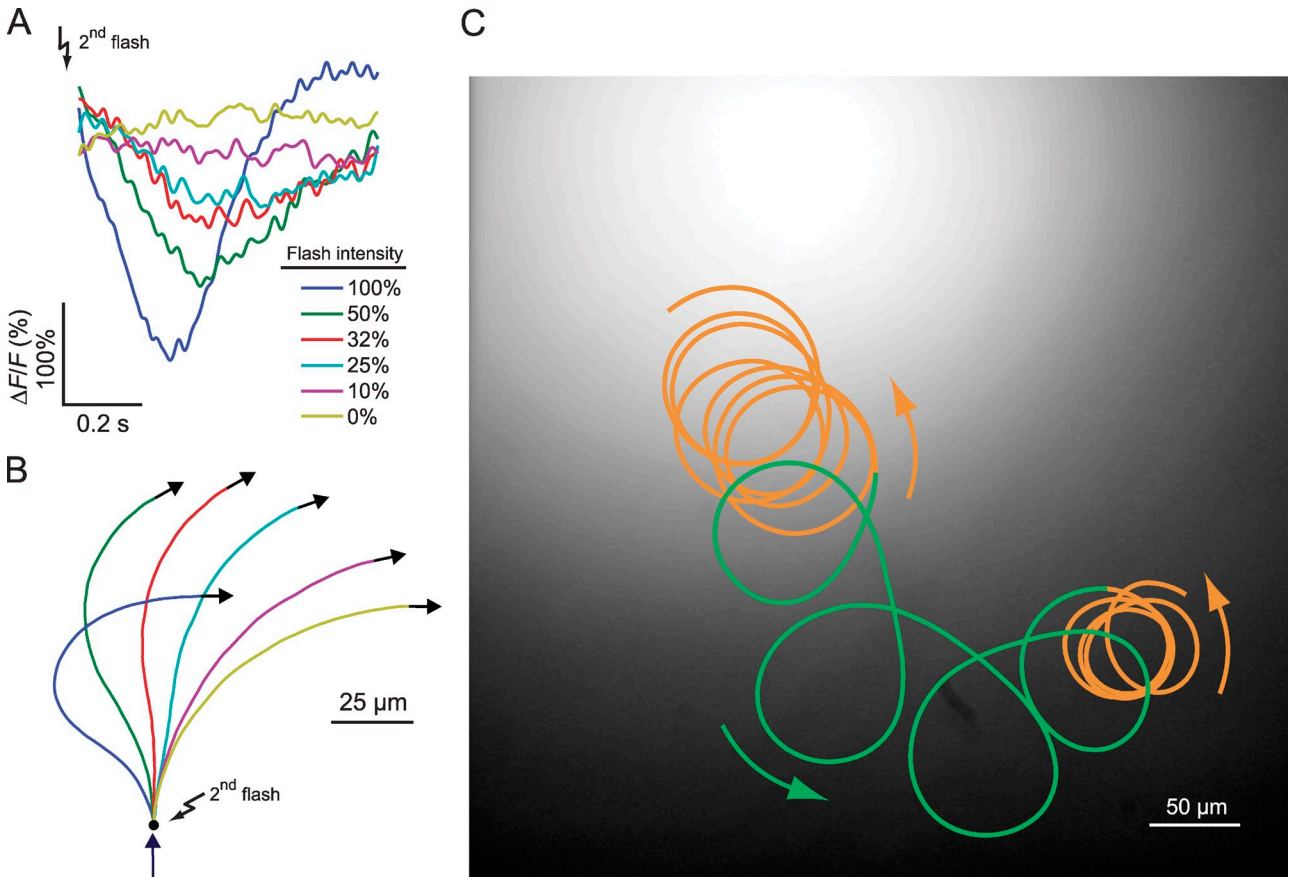

Figure 6. **Functional implications of the Ca^{2+} drop.** (A) Ca^{2+} signals derived from the data in Fig. 3 C. The amplitude of Ca^{2+} signals was rescaled to match the mean amplitude of single-cell Ca^{2+} signals. (B) Swimming paths reconstructed from Ca^{2+} signals in part A. Arrow indicates the swimming direction shortly before the second flash. (C) Sperm swimming in a gradient of resact. The UV profile used for uncaging resact is shown in shades of gray. At the foot and on the top of the gradient, the cell swims on smooth drifting circles (orange). In the region where the gradient is steep, the cell swims on looping trajectories (green). Arrows indicate the swimming direction.

path after the second flash by using population Ca^{2+} signals (Fig. 6). This is feasible because sperm from sea urchins, unlike mammals, are considered a homogenous population.

We studied how the intensity of the second flash (Fig. 3 C) shapes the overall Ca^{2+} signal and, thereby, the swimming path. For a strong second flash, the Ca^{2+} drop was steep, whereas for a weak flash, it was shallower (Fig. 6 A). The swimming response to the second flash graded with flash intensity: during the Ca^{2+} drop, $\kappa(t)$ became gradually smaller, i.e., cells extended the "run" period toward the source (Fig. 6 B, e.g., compare red and yellow paths). For strong flashes, the steep Ca^{2+} drop even resulted in a change of sign of $\kappa(t)$ (Fig. 6 B, green and dark blue), similar to paths observed for single cells. The subsequent turn also depended on the intensity of the second flash; if the second flash is strong, the Ca^{2+} rise is also steep, resulting in a sharp turn. The overall trajectory will be highly bent, reminiscent of the looping trajectories (wide arcs and sharp turns) often observed in the swimming of marine invertebrates during chemotaxis. However, when the second flash is weaker, the Ca^{2+} rise after the drop is also weaker, leading to a smoother turn, which gives rise to smoothly drifting circles.

We compared these reconstructed trajectories with a trajectory of a sperm cell swimming in a chemoattractant gradient (Fig. 6 C). We observe a sequence of successive "turn and run" events that eventually direct the sperm to the center of the gradient. Far away and close to the chemoattractant source, the gradient is shallow, and therefore, stimulation of sperm is weak. The trajectory is composed of a series of slowly drifting circles (Fig. 6 C, orange). When the cell swims up the gradient (Fig. 6 C, green), stimulation is stronger, the run periods toward the source are longer, and the subsequent turns are more pronounced. We propose that a second stimulation during a run period initiates a Ca^{2+} drop that prolongs the swimming path along the direction of the gradient. Moreover, the run period is an active process that depends on the stimulus strength.

Recovery from stimulation and adjustment of sensitivity

During chemotaxis, sperm are exposed to chemoattractant concentrations spanning several orders of magnitude. How do sperm adjust their sensitivity accordingly? We probed sperm's sensitivity to stimuli delivered on top of different background concentrations. For example, a pulse of 100 pM resact resulted in a free concentration of ~400 fM calculated accordingly (Eq. 3; Fig. 7 A). For Δt ranging from 0.4 to 15.4 s, the sensitivity was probed with ~30 pM released from caged resact (Fig. 7 A). For short Δt, the test V_m signal was strongly attenuated; however, for longer Δt, it progressively recovered. For $\Delta t \geq 8$ s, ΔV_m became

Published September 17, 2012

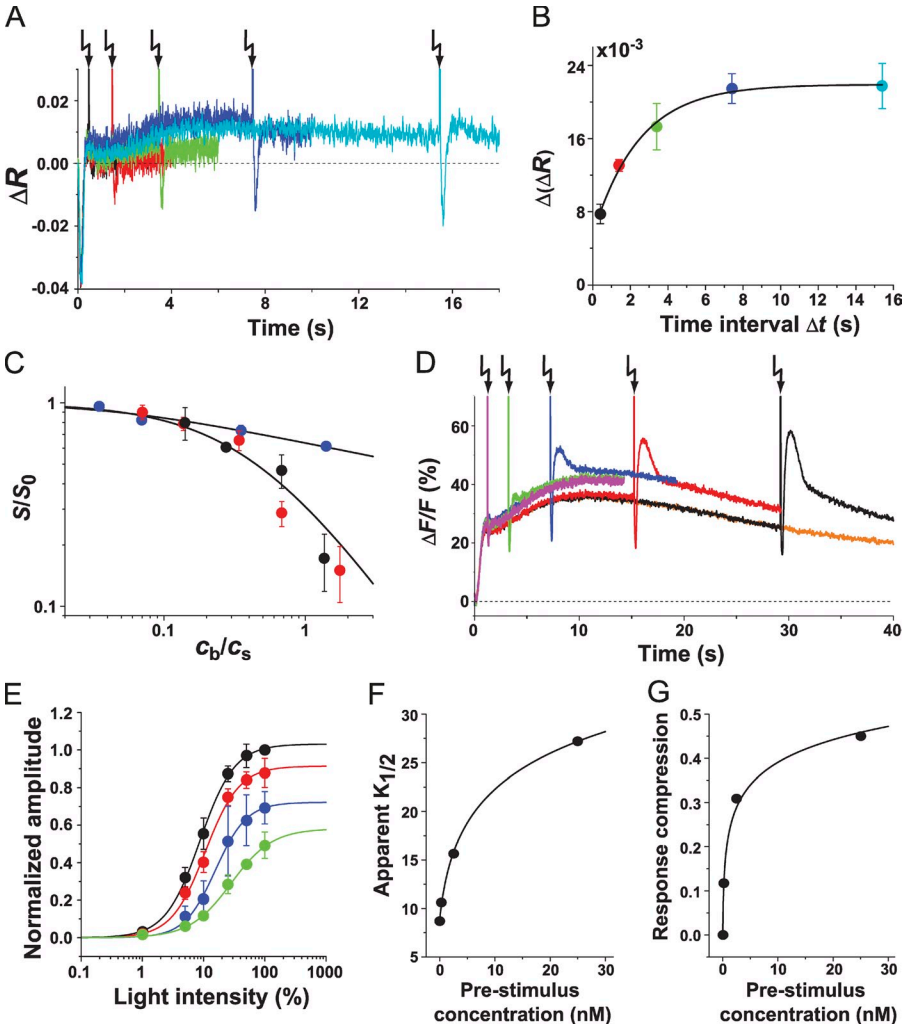

Figure 7. **Adaptation of V_m and Ca^{2+} signals.** (A) Adaptation and recovery of the V_m signal after an adapting stimulus. Sperm were mixed with 100 nM caged resact, equivalent to 100 pM resact because of the "residual" activity of caged resact. The final free resact concentration was ~400 fM. Sperm were probed with a test stimulus (100% flash; releasing ~30 pM resact) at different Δt (in seconds): 0.4 (black), 1.4 (red), 3.4 (green), 7.4 (blue), and 15.4 (cyan). (B) Recovery kinetics of the V_m signal as shown in A ($n = 3$; color coding as in A). The data points were fit with an exponential curve ($R^2 = 0.99$). (C) Weber–Fechner plot. Sperm were adopted by background concentrations c_b of 0.27, 2.1, 4.1, 10.1, 20.4, and 52.5 pM. Test stimuli c_b of either resact or cGMP were given. 15 pM (black symbols) or 30 pM (red symbols) resact (c_s) was released from caged resact. The voltage response $S = \Delta V_m$ was normalized to the value in the absence of background S_0 and plotted versus the concentration ratio $R = c_b/c_s$. Similarly, test stimuli of cGMP were probed (blue symbols). Solid lines were calculated using either Eqs. 1 or 2, respectively (resact, $n = 3$ and cGMP, $n = 4$). (D) Ca^{2+} signals evoked by a test stimulus of cGMP at different Δt of (in seconds): 1.2 (magenta), 3.2 (green), 7.2 (blue), 15.2 (red), and 29.2 (black). Ca^{2+} signal evoked by 4.1 pM background resact alone is shown in orange. (E) Shift of the dynamic range of Ca^{2+} signals. Test stimuli of cGMP ($\Delta t = 15.2$ s) were given either in the absence (black) or presence of adapting resact (in nanomolars): 0.25 (red), 2.5 (blue), and 25 (green). Ca^{2+} signal amplitudes produced by a test cGMP stimulus were plotted; in the presence of background resact, the Ca^{2+} signal amplitude was the difference between the value before the test stimulus and the value at the minimum of the Ca^{2+} drop. The data were fitted with the equation

$$A = A_{max}\frac{I^n}{I^n + K_{1/2}^n},$$

wherein A is the response amplitude, I denotes the flash intensity, and n is the Hill coefficient. (F and G) Apparent $K_{1/2}$ (F) and response compression (G) at different background concentrations. Data are obtained from E. Error bars show SDs. Arrows indicate time of flashes.

constant, showing that sperm had reached a stable sensitivity (Fig. 7 B). Next, sperm were exposed to background concentrations (c) ranging from ~2 to 50 pM. The sensitivity was tested after 8 s (Fig. 7 C). The scaled sensitivity (S/S_0) as function of background to test stimulus ratio, $R = c_b/c_s$ (Fig. 7 C), was fitted with the Weber–Fechner relation (Matthews et al., 1990)

$$S/S_0 = \left(1 + \frac{R}{R_{1/2}}\right)^{-1}, \quad (1)$$

in which $R_{1/2}$ represents the concentration ratio for half-maximal desensitization. $R_{1/2}$ adopted a value of 0.44; thus, to obtain a 50% response, the test concentration has to be approximately twice (200%) as large as the background concentration.

A likely site of desensitization is the receptor. To dissect receptor desensitization from downstream events, the receptor was bypassed using cGMP as the test stimulus. Sperm were first stimulated with resact followed by a pulse of cGMP to probe the sensitivity. The flash intensity was adjusted such that, in nonadapted sperm, the ΔV_m evoked by 30 pM resact or by release of cGMP was similar. Desensitization was much less pronounced when the receptor was bypassed (Fig. 7 C). Data were described by a modified Weber–Fechner relation (Matthews et al., 1990),

$$S/S_0 = \left(1 + \frac{R}{R_x}\right)^{-\alpha}, \quad (2)$$

with $\alpha = 0.14$ and $R_x = 0.04$. Using these parameters, $R_{1/2}$ was 5.6; thus, to obtain a 50% response, only a 20% increase of concentration over background is required. In conclusion, a large portion of desensitization takes place at the receptor level.

Published September 17, 2012

Many sensory systems such as photoreceptors (Laughlin, 1989), hair cells (Eatock et al., 1987; Peng et al., 2011), olfactory sensory neurons (Kurahashi and Menini, 1997; Kleene, 2008), or bacteria during chemotaxis (Mesibov et al., 1973; Vladimirov and Sourjik, 2009) respond over a broad range of stimulus strength by shifting their sensitivity. Therefore, we determined the relation between stimulus strength and Ca^{2+} signal amplitude at various background concentrations. Fig. 7 D shows an example of Ca^{2+} signals evoked at different Δt for a background concentration of 4.1 pM resact. The dose–response relation at various background concentrations was measured by delivering the cGMP test pulse (Δt = 15.2 s). In the presence of a background, the dose–response relation was shifted to higher levels of stimulation, i.e., $K_{1/2}$ increased, and the Ca^{2+} response was compressed (Fig. 7, E–G). In summary, several hallmarks of adaptation in sensory cells—Weber–Fechner law, response compression, and a shift of the dynamic range—operate in sperm.

Range of sperm attraction

An important question concerns the effective range of a chemical gradient. The range can be estimated from the concentration profile formed by radial diffusion of resact from an egg. To numerically calculate the gradient, we determined (a) the amount of resact released by *A. punctulata* eggs and (b) the diffusion coefficient of resact.

We determined the amount of resact released from eggs suspended in artificial sea water (ASW) for 60 min. The resact concentration was measured by comparing the Ca^{2+} responses of Fluo-4–loaded sperm evoked by appropriately diluted aliquots of egg-conditioned ASW and by resact standards. Taking the egg volume into account, the amount of released resact (2.75×10^{-14} mol or 1.65×10^{10} molecules/egg) corresponded to a concentration in the egg of 50 ± 25 µM (n = 8).

The diffusion coefficient of dye-labeled resact (Alexa Fluor 488–resact; $D_{labeled}$) determined by two-focus fluorescence correlation spectroscopy (Fig. 8 A; Dertinger et al., 2007, 2008) was 231 ± 7 µm^2/s (n = 9). D_{resact} of the unlabeled peptide was calculated to be 239 ± 7 µm^2/s (see Materials and methods).

Using the two measures, we simulated how the concentration profile of resact, diffusing from an egg on a planar floor, develops with time (Fig. 8 B). The profile 20 µm above the floor at first is narrow and steep; with time, it becomes broader and shallower. Within 20 min after egg release, the peak concentration dropped from 50 µM to <10 nM (Fig. 8 C).

The maximum attraction range was estimated using two criteria: (1) the minimal number of resact molecules absorbed per unit of time (N_{abs}) that evoke a Ca^{2+} signal and (2) the minimal steepness of a gradient (g_{min}) that can be registered by sperm (see Materials and methods). To define the first criterion, we assumed that a single resact molecule absorbed during a swimming circle is sufficient. This criterion corresponds to a concentration c_{min} = 44 fM. The distance from the egg, where this resact concentration is established, can adopt values ≤5 mm (Fig. 8 C).

The second criterion, g_{min}, is based on the assumption that the number of absorbed molecules, N_{abs}, is equal or larger than the noise as a result of statistical fluctuations $\sqrt{N_{abs}}$, i.e., the *S/N* ratio ≥ 1 (see Materials and methods). For the single-molecule regimen (c_{min} = 44 fM), the limiting g_{min} = 0.8 fM/µm. Using g_{min} and the simulated gradient, we estimated the maximal distance from which sperm can be attracted. For different times after the release of resact, we calculated the gradient dc/dx versus distance x from the egg (Fig. 8 E). For comparison, the respective minimal gradients, g_{min}, are also shown (Fig. 8 E). Attraction is supported in regions with gradients steeper than g_{min}. For times t = 1, 2, 5, 10, 20, and 60 min, the effective range is 1.0, 1.3, 1.9, 2.6, 3.3, and 4.7 mm, respectively. Fig. 8 F shows the effective range of attraction versus time after egg release. We used the gradient estimate after 10 min to determine the number of bound resact molecules per flagellum for sperm swimming on circular paths at various distances from the egg (Fig. 1 C). The time course nicely illustrates that circular swimming in a gradient causes a periodic modulation of the number of absorbed molecules.

For long times (t > 30 min), the resact gradient near the egg becomes shallower than g_{min} (Fig. 8, E and F), and sperm might struggle to locate the egg. Therefore, we envisioned an alternative scenario for which eggs continue to produce resact after the release. Assuming a synthesis rate of 10^3 resact molecules/s, the effective range adopts identical values for the respective times t. However, in the vicinity of the egg, the resact gradient is steeper than g_{min} even after 60 min (Fig. 8 G). Thus, moderate resact synthesis supports sperm attraction near the egg.

Discussion

Sperm navigating in a chemical gradient are exposed to a stream of chemoattractant molecules that is modulated by the periodic movement of sperm and translated into Ca^{2+} oscillations. Here, we identify three principles that govern gradient sensing in sperm, sampling, resetting, and adaptation, and we model the range of gradient detection.

Sperm temporally sense a chemical gradient

Cells exploring a chemical gradient use either spatial or temporal sampling (Dusenbery, 2009). For spatial sensing, cells compare concentrations along the body length. For temporal sensing, cells probe the concentration in time as they move from one place to another. Usually, large and slowly moving cells use spatial sensing, whereas small and rapidly moving cells use temporal sensing (Iglesias, 2012). Sperm are large and fast moving; hence, it is not straightforward to predict the sensing mechanism. Previous studies provided clues that sperm use a temporal rather than a spatial mechanism (Strünker et al., 2006): the CNGK channel is distributed over the entire length of the flagellum (Bönigk et al., 2009), and hyperpolarization—the principal electrical signaling event—is expected to spread within a few milliseconds along the flagellum (Hille, 2001); thereby, spatial information is blurred. To distinguish between spatial and temporal mechanisms, an experimental test is to inflict a temporal stimulus pattern independent of a cell's position (Dusenbery, 2009). Using this approach, we show that sperm

Published September 17, 2012

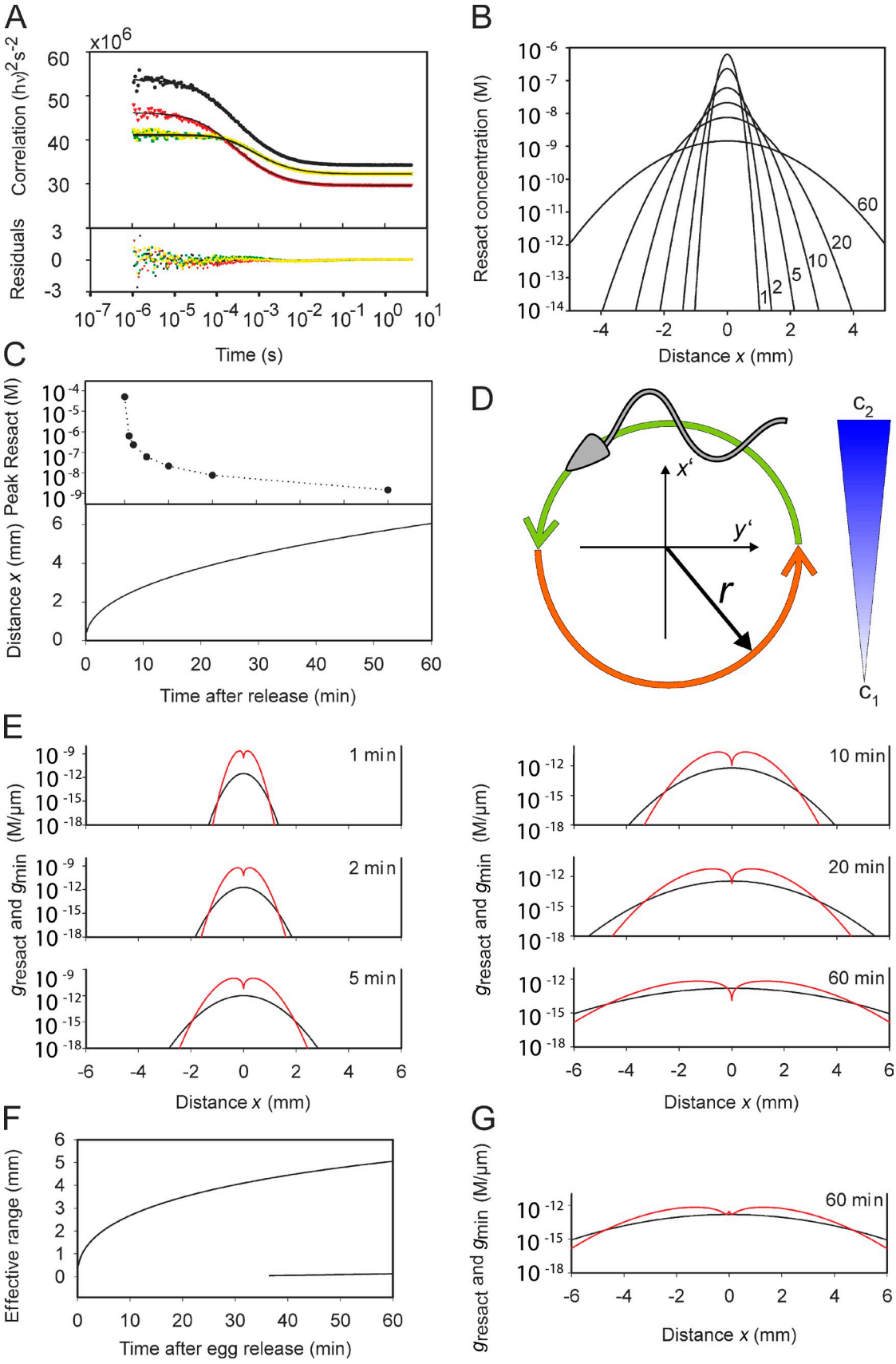

Figure 8. **Range of sperm attraction.** (A) Determination of the diffusion coefficient of resact by two-focus fluorescence correlation spectroscopy. Resact was labeled at Cys 1 with Alexa Fluor 488 dye. The autocorrelation function of the first focus (black), the second focus (red), and the cross correlation of both foci (yellow and green) are shown. Symbols are experimental data points, and solid lines are global fits using three fit parameters (see Materials and methods).

Published September 17, 2012

temporally sample chemoattractant molecules and translate a spatial concentration pattern into a temporal Ca^{2+} pattern.

The reliability of gradient detection increases proportionally to the square root of the sampling time (Berg and Purcell, 1977). However, for long sampling times, important spatial features of the concentration profile might be missed. Thus, what might be an optimal sampling time that reconciles high sensitivity with sufficient spatial resolution? During a sampling time of 0.2–0.6 s, sperm advance 36–108 µm (swimming speed 180 µm/s), i.e., sperm sample molecules along a path that roughly equals one body length or up to half the circumference of a swimming circle. Sampling is optimal if the whole cell surface is exposed to a different concentration during the sampling time (Dusenbery, 2009). Therefore, the precision by which sperm map a spatial pattern of chemoattractants is about one body length. In summary, circle diameter, swimming speed, and sampling time are perfectly tuned to achieve optimal gradient sensing.

During the short sampling time, bound and free resact are not in chemical equilibrium. Consequently, sperm register changes in the rate of binding events rather than absolute chemoattractant concentrations as, for example, in the worm *Caenorhabditis elegans* (Lockery, 2011). In a similar vein, the mechanical response of the flagellum is encoded by $d[Ca^{2+}]/dt$ rather than absolute $[Ca^{2+}]_i$ (Alvarez et al., 2012). This mechanism is distinctively different from bacterial chemotaxis, in which receptor occupancy matters rather than the rate of changes in occupancy (Sourjik and Armitage, 2010). For bacteria, chemoattractant concentrations and dissociation constant (K_d) values are in the micromolar range, and therefore, free and bound chemoattractants are almost instantaneously in chemical equilibrium on the time scale of the chemotactic response. An important insight of this and a previous study (Alvarez et al., 2012) is that measuring rates of binding events rather than absolute concentrations might be an evolutionary adaptation to extremely low chemoattractant concentrations.

A general concept of temporal sampling implies that sperm take two brief samples separated by Δt, calculate a concentration difference Δc, and then respond. In precise terms, however, temporal sampling is different. Sperm sample chemoattractant molecules until Ca^{2+} channels open. The ensuing steering response is encoded by the Ca^{2+} dynamics (Alvarez et al., 2012). The waveform of Ca^{2+} pulses will be entirely different for steep versus shallow gradients; accordingly, sperm will follow different paths.

We found that the sampling time relates inversely to the stimulus strength. With increasing chemoattractant concentration, the sampling time shortens. The shortening can be considered as one of several mechanisms of adaptation that prevent sperm from response saturation.

Reset mechanism

A second stimulus, delivered during an ongoing Ca^{2+} signal, resets the cell. The reset mechanism probably involves closure of Ca_v channels and Ca^{2+} extrusion via NCKX exchange. During reset, a new phase relation between stimulus and response functions is established. In a generic model of sperm chemotaxis, a periodic stimulation is translated into a periodic modulation of path curvature (Friedrich and Jülicher, 2007). A key feature of this mechanism is that the phase relation between stimulus and response functions determines the swimming direction. The phase is primarily determined by the latency of the Ca^{2+} signal. Although cruising in continuous, shallow gradients, the reset mechanism will entrain Ca^{2+} oscillations with the angular frequency of circular swimming and, therefore, couple periodic stimulation to a periodic response. When sperm encounter a chemoattractant surge in a discontinuous chemoattractant field, the reset might establish a new phase relation.

Sperm can encode periodic stimuli

Sperm track changes in resact concentration with ~1 Hz, i.e., the angular frequency of circular swimming. Quite remarkably, at low chemoattractant concentrations, sperm can generate V_m responses at a frequency of <1 Hz with no sign of adaptation. This finding implies that CNGK channels faithfully translate periodic cGMP changes into a train of hyperpolarizing V_m pulses. The slower Ca^{2+} signals, however, do not recover completely between spikes. As a result, Ca^{2+} signals of equal amplitude are superimposed on a steady Ca^{2+} level. What might be the functional consequences of such a Ca^{2+} response pattern? The path curvature κ follows on the heels of $d[Ca^{2+}]_i/dt$ to produce a quick steering response (Alvarez et al., 2012). However, κ also changes on a longer timescale (Böhmer et al., 2005; Alvarez et al., 2012). The signaling events underlying the long term changes in κ are not known. The steady-state Ca^{2+} level might be one of several factors (Alvarez et al., 2012).

Mechanism of adaptation

The exquisite sensitivity enables sperm to sample each and every binding event to produce a response. At the same time, sperm must cope with a broad range of resact concentrations, which poses a formidable challenge of avoiding response saturation at various stages along the chemomechanical transduction pathway. To tackle similar problems, sensory systems have engineered appropriate mechanisms to modulate their sensitivity (Torre et al., 1995; Burns and Baylor, 2001; Kleene, 2008; Vladimirov and Sourjik, 2009). For example, eight distinct mechanisms control light adaptation in vertebrate photoreceptors (Pugh et al., 1999).

Residuals are shown on the bottom. (B) Shape of the resact gradient from a single *A. punctulata* egg for different times (1–60 min) after egg release. (C, top) Peak resact concentration at the center of release for different times after egg release. (bottom) Distance from the egg at which a cell captures one resact molecule during a swimming circle. (D) Cartoon of circular swimming of sperm in a chemoattractant gradient. The concentration of resact (blue) increases linearly from c_1 to c_2 during a complete circle. The cell compares the concentration of resact bound along both semicircles and computes the difference ΔN_{abs}. (E) Resact gradient (black) and the minimal gradient g_{min} (red) for the indicated times after egg release. For the effective range of sperm attraction, the resact gradient must be larger than g_{min}. (F) Effective range of sperm attraction versus time after egg release. At $t > 30$ min, $g_{resact} \leq g_{min}$ in the very vicinity of the egg. Hence, we observe two boundaries, a short one and a long one for the effective gradient. (G) Resact gradient g_{resact} (black) and minimal gradient g_{min} (red) for an egg that synthesizes 1,000 resact molecules/s. 60 min after egg release, the range of attraction is similar to that for an egg with no synthesis. However, near the egg, $g_{resact} > g_{min}$ even after 60 min.

Published September 17, 2012

In sperm, premature response saturation is prevented by shifting the sensitivity range to higher resact concentrations and by compressing the Ca^{2+} signal. The different Weber–Fechner relations for resact/resact and resact/cGMP paired-stimulus experiments argue that a major adaptation site is the GC receptor itself. The GC might be desensitized by dephosphorylation (Ward and Vacquier, 1983; Vacquier and Moy, 1986) or other feedback mechanisms. For example, in photoreceptors, Ca^{2+} feedback controls cGMP synthesis by GC (Koch and Stryer, 1988; Pugh et al., 1999; Pugh and Lamb, 2000). In photoreceptors and olfactory neurons, Ca^{2+} feedback shuts down CNG channels and, thereby, terminates the response (Hackos and Korenbrot, 1997; Rebrik and Korenbrot, 2004; Rebrik et al., 2012). However, the CNGK channel faithfully tracks changes in cGMP concentration even at high Ca^{2+} levels.

Finally, a novel mechanism of perfect adaptation has been discovered that allows sperm to maintain their mechanical responsiveness even at high Ca^{2+} levels. The path curvature κ depends on $d[Ca^{2+}]/dt$ rather than $[Ca^{2+}]_i$ (Alvarez et al., 2012). Consequently, even small modulations of $[Ca^{2+}]_i$ on top of a high quasi steady-state Ca^{2+} level can evoke a steering response.

In summary, we envisage several distinct mechanisms that regulate the responsiveness of sperm. Future studies should address adaptation in quantitative terms.

Minimal gradient and effective range of gradient

The single-molecule sensitivity allows estimation of a minimal gradient of 0.8 fM/µm that can be detected by sperm. With 50 µM resact in the egg, the effective range of the gradient can be ≤4.7 mm. The ratio of egg volume to volume demarcated by the effective range illustrates that chemotaxis enhances the probability to reach an egg by $\sim 10^6$-fold. Sperm sensitivity is unique compared with other chemotactic cells, such as bacteria and *Dictyostelium discoideum*. A lower bound for gradient sensitivity in bacteria, depending on the sensitivity of the receptor, ranges between 0.5 and 62 nM/µm (Kalinin et al., 2009; Neumann et al., 2010). The response thresholds of *A. punctulata* sperm for resact is ∼100 fM, of bacteria for aspartate ∼10 nM (Mao et al., 2003), and of *D. discoideum* for cAMP ∼1 nM (Wang et al., 2012). Probably, g_{min} scales with the ligand affinity of the chemoattractant receptor.

The effective range is similar for scenarios with and without chemoattractant synthesis. However, the situation might be different when strong shear alters the chemoattractant distribution (Riffell and Zimmer, 2007; Zimmer and Riffell, 2011). Under such conditions, the chemoattractant is washed away, and the gradient is determined by the synthesis rate and the flow field around the egg (Zimmer and Riffell, 2011). Although turbulence in the case of broadcast spawners is beneficial for gamete mixing, it unfavorably affects the spatiotemporal pattern of the gradient. The length scale for which mass transport is dominated by diffusion is the Kolmogorov length; it typically ranges between 1 and 6 mm in the ocean (Lazier and Mann, 1989). Although turbulence might set an additional limit for the range of sperm attraction, the similar scale of the effective gradient range and the Kolmogorov length argues that turbulence might not be a critical factor in chemotaxis of sea urchin sperm.

Although several of our assumptions are plausible, arguably some are arbitrary. For example, we do not know the *S/N* level at which sperm operate. Moreover, N_{abs} is a measure of the number of molecules that hit the flagellum; how many of those molecules are captured by the receptor is unknown. Finally, freely swimming sperm follow a gradient on a helical path (Crenshaw and Edelstein-Keshet, 1993; Corkidi et al., 2008) and not on drifting circles. Future work should address gradient sensing of single cells in 3D using caged chemoattractants to quantitatively sculpture chemical gradients by light and to follow the swimming behavior in real time.

Summary

We unveil several mechanisms that enable sperm to probe a chemical gradient intermittently and, thereby, transduce a stream of molecules into discrete Ca^{2+} signals while maintaining a high sensitivity over a remarkably wide concentration range. Sperm from other marine invertebrates (Matsumoto et al., 2003; Shiba et al., 2008; Guerrero et al., 2010b, 2011) also swim on drifting circles that are controlled by periodic Ca^{2+} signals. Aside from sperm, many cellular organisms are propelled on periodic paths by cilia or flagella during chemotaxis and phototaxis (Brokaw, 1959; Thar and Fenchel, 2001; Jékely et al., 2008; Jékely, 2009). Our work provides a conceptual framework of mechanisms—stimulus sampling, reset, and adaptation—that might be helpful to study gradient sensing in other eukaryotic cells.

Materials and methods

Materials and solutions

A. punctulata were obtained either from M.L. Wise (Duke University Marine Laboratory, Beaufort, NC) or the Marine Resource Center, Marine Biological Laboratory. *S. purpuratus* were obtained from P. Leahy (Kerckhoff Marine Laboratory, Corona Del Mar, CA). Animals were maintained in seawater tanks at 14°C with constant aeration and algal food. The collection of "dry" sperm from male sea urchins and the composition of ASW were as described previously (Kaupp et al., 2003). In brief, we injected ∼200 µl of 0.5-M KCl (Palmer, 1937) in the body cavity or applied electrical stimulation using lead electrodes at a potential of 25 V peak to peak to the sea urchins at any two points on the shell of the animal (Harvey, 1954). The spawned sperm (dry sperm) was collected in an Eppendorf tube using a Pasteur pipette and stored on ice. The experiments were performed on the same day. In a similar way, we obtained eggs from female sea urchins. ASW, pH 7.8, contained 423 mM NaCl, 9 mM KCl, 9.27 mM $CaCl_2$, 22.94 mM $MgCl_2$, 25.5 mM $MgSO_4$, 0.1 mM EDTA, and 10 mM Hepes.

Preparation of sperm flagella membrane proteins

To obtain a pure preparation of flagella (both for sperm of *A. punctulata* and *S. purpuratus*), 1 ml of dry sperm was diluted in 24 ml ASW and centrifuged (200 *g* for 7 min) to sediment coelomocytes. The supernatant was removed and centrifuged (3,000 *g* for 15 min) to sediment sperm. The sperm pellet was resuspended in 10 vol ASW with a mammalian tissue protease inhibitor cocktail (mPIC; Sigma-Aldrich; 1:100 dilution in ASW). The sperm suspension was sheared 20–25 times on ice with a 20-gauge needle. The sheared suspension was centrifuged (2,000 *g* at 4°C for 10 min). Flagella remained in the supernatant, and intact sperm or sperm heads formed the pellet. The purity of flagella preparations was checked using phase-contrast microscopy. This procedure was repeated twice. The flagella pellets were stored at −80°C until further use.

Membrane proteins from *A. punctulata* sperm flagella were prepared by the pH 9.2 method as described previously (Mengerink and Vacquier, 2004; Strünker et al., 2006). In brief, an equal volume of ASW at pH 9.2 (40 mM Tris base, pH 9.2, 10 mM benzamidine-HCl in ASW, and 1:100 dilution of mPIC) was added slowly to the flagella suspension while stirring. The suspension was kept at 4°C overnight. The suspension was

Published September 17, 2012

stirred vigorously for 5 min using a magnetic stirrer. Two centrifugation steps were used to remove the cell debris (6,000 *g* for 4°C at 30 min). The supernatants that contained membrane vesicles were combined. The vesicles were sedimented by a final centrifugation step (100,000 *g* at 4°C for 60 min). The membrane pellets were stored at −80°C. Finally, pellets were resuspended in isotonic buffer (150 mM NaCl, 5 mM EDTA, 10 mM Tris/HCl, pH 7.4, 2 mM DTT, and 1:500 dilution of mPIC), solubilized using SDS sample buffer, and subjected to standard SDS-PAGE.

We made a detergent-based protein preparation from the flagella of *S. purpuratus* sperm. Flagella pellets were dissolved in PBS containing 2 mM EDTA and 1:500 mPIC (PBS++). An equal volume of PBS++ containing 20 mM *n*-dodecyl-β-maltoside (Anatrace) was added while stirring. The suspension was incubated for 60 min on ice with occasional vortexing. Afterward, the suspension was centrifuged (14,000 rpm at 4°C for 30 min), and the supernatant was collected. Such a protein preparation was subjected to standard SDS-PAGE.

Mass spectrometric identification of proteins

After separating membrane proteins by standard SDS-PAGE, we performed tryptic in-gel digestion and liquid chromatography tandem mass spectrometry analysis as previously described (Strünker et al., 2006). In brief, gel slices were washed with 50% (vol/vol) acetonitrile in 25 mM ammonium bicarbonate, shrunk by dehydration in acetonitrile, and dried in a vacuum centrifuge. The gel pieces were reswollen in 10 µl ammonium bicarbonate (50 mM) containing 50 ng trypsin (sequencing grade modified; Promega). After 17-h incubation at 37°C, the enzymatic reaction was terminated by addition of 10 µl of 0.5% (vol/vol) trifluoroacetic acid (TFA) in acetonitrile, and the separated liquid was taken to dryness under vacuum. Samples were reconstituted in 6 µl of 0.1% (vol/vol) TFA and 5% (vol/vol) acetonitrile in water. For identification of *A. punctulata* proteins, tryptic peptides were separated on a liquid chromatography system (CapLC; Micromass) equipped with capillary column (3 µm, 100 Å, 150 mm × 75 µm inner diameter [i.d.]; PepMap C18; Dionex). Mass spectrometry and tandem mass spectrometry were performed on a quadrupole orthogonal acceleration time-of-flight mass spectrometer (Q-TOF Ultima; Micromass). Preparations from the flagella of *S. purpuratus* sperm were analyzed using an Orbitrap mass spectrometer (LTQ Orbitrap XL; Thermo Fisher Scientific) equipped with a 2D nanoflow liquid chromatography system (Eksigent; Axel Semrau GmbH) as previously described (Lange et al., 2010). 6 µl of the peptide sample was injected and concentrated on a trap column (5 µm, 100 Å, 5 mm × 300 µm i.d.; PepMap C18) equilibrated with 0.1% TFA and 2% acetonitrile in water. After switching the trap column in line, liquid chromatography separations were performed on a capillary column (3 µm, 100 Å, 150 mm × 75 µm i.d.; Atlantis dC18; Waters) at an eluent flow rate of 250 nl/min using a linear gradient of 0–40% B in 80 min. Mobile phase A was 0.1% formic acid (vol/vol) in water; mobile phase B was 0.1% formic acid in acetonitrile. Data were acquired in a data-dependent mode using one mass spectrometry scan followed by tandem mass spectrometry scans of the most abundant peaks. The processed tandem mass spectrometry spectra and the MASCOT server version 1.9 and 2.2 (Matrix Science) were used to search in house against the NCBI nonredundant protein database. The maximum of two missed cleavages was allowed, and the mass tolerance of precursor and sequence ions was set to 100 ppm and 0.05 D, respectively. For the LTQ Orbitrap measurements, the mass tolerance of precursor and sequence ions was set to 10 ppm and 0.35 D, respectively. Methionine oxidation and the acrylamide modification of cysteine were used as variable modifications. A protein was accepted as identified if at least two tryptic peptide scores indicated identity or extensive homology.

Measurement of changes in V_m and $[Ca^{2+}]_i$

Resact- and cGMP-induced changes in V_m and $[Ca^{2+}]_i$ were measured with a voltage-sensitive dye (Di-8-ANEPPS; Molecular Probes) and a fluorescent Ca^{2+} indicator (Fluo-4 AM; Molecular Probes), respectively, in a stopped-flow device (SFM-400; Bio-Logic) as described previously (Strünker et al., 2006; Bönigk et al., 2009). In brief, dry sperm was suspended 1:6 (vol/vol) in loading buffer containing ASW, fluorescence dye, and 0.5% Pluronic F127 (Sigma-Aldrich or Molecular Probes). After incubation (for 45–120 min with Fluo-4 AM and 5 min for Di-8-ANEPPS) at 17°C, the sample was diluted 1:20 with ASW. Sperm were allowed to equilibrate in the new medium for 5 min. In the stopped-flow device, the sperm suspension was rapidly mixed 1:1 (vol/vol) with the respective stimulants. Fluorescence was excited by a 150-W Xe lamp (LSB521; LOT-Oriel GmbH & Co. KG). Emission was recorded by a photomultiplier module (H9656-01 or H9656-20; Hamamatsu Photonics). The signal was amplified and filtered through a voltage-amplifier (DLPVA-100-B-S; Femto Messtechnik GmbH). Data acquisition was performed with a data acquisition pad (PCI-6221; National Instruments) and Bio-Kine software v. 4.49 (Bio-Logic). For Ca^{2+} and V_m recordings, the excitation light was passed through a filter set containing either two GG-435 (Andover Corporation) and two FITCA-40 (Schott) filters or two GG-435 and an ET490/20× filter (Chroma Technology Corp.). For Ca^{2+} measurements, the emitted light was passed through a BrightLine 525/40 filter (Semrock). Ca^{2+} signals represent the average of at least three recordings and are depicted as the percent change in fluorescence. The V_m signals were recorded in the dual-emission mode. The filters in front of the two photomultiplier modules were HQ535/30m (Chroma Technology Corp.) and HQ580/40m (Chroma Technology Corp.). The ΔR was derived as previously described (Strünker et al., 2006). In brief, the Bio-Logic software enabled recording of fluorescence in the ratiometric dual-emission mode. The V_m signals are the ratio of F_{535}/F_{580} or R. The control (ASW) R signal was subtracted from the resact- or cGMP-induced signals. The R value before the onset of the changes in fluorescence was set to 0, yielding ΔR. The V_m signals represent the average of at least five recordings and were digitally smoothed with five point average smoothing. The data obtained from the stopped-flow recordings were analyzed using either Prism 5 (GraphPad Software) or OriginPro 8.1G SR3 (OriginLab Corporation).

Caged compounds and flash photolysis

All caged compounds were obtained from V. Hagen (Leibniz-Institut für Molekulare Pharmakologie, Berlin, Germany; Hagen et al., 2001, 2002, 2003; Kaupp et al., 2003). We incubated sperm with 30 µM DEACM-caged cGMP for ≥45 min (Kaupp et al., 2003). Caged cGMP and caged resact were photolyzed by a flash of ∼1 ms of ultraviolet light from a Xenon flash lamp (JML-C2; Rapp OptoElectronic). The flash of light was passed through a band pass 295–395 interference filter (Rapp OptoElectronic) and delivered by a liquid light guide to the cuvette (FC-15; Bio-Logic) of the stopped-flow device. The flash lamp contained two capacitors of 1,000 µF each, which can be charged to a maximum of 385 V. The two capacitors can be triggered independently giving identical energy output, in principle, at the same time or separated by a few milliseconds to several seconds. The flash energy was measured using a pyroelectric sensor (JM20; Rapp OptoElectronic). When the capacitors where charged at 300 V, the flash energy at the end of the light guide was 6.5 mJ. For caged resact experiments, we charged the capacitors to 300 V, whereas for caged cGMP experiments to 150 V. The flash energy was further adjusted using calibrated neutral density filters (Rapp OptoElectronic). The neutral density filters were housed in a filter wheel (Rapp OptoElectronic). The position of the filter wheel at different flashes as well as the triggering and timing of flashes during acquisition were defined through the interface of a self-made program written in LabVIEW 8.0 (National Instruments).

Simulation of the stimulus function during stopped-flow experiments

The kinetics of the binding reaction was solved numerically by direct integration of the mass balance equation. Changes in the free concentration of resact and GC were calculated iteratively using the expression

$$[resactGC]_{t+\Delta t} = [resactGC]_t + ([resact]_t[GC]_t k_{on} - [resactGC]_t k_{off})\Delta t, \quad (3)$$

in which [*resact*] and [*GC*] represent the respective free concentrations. The integration time step Δt was 1 ms. We assumed 10^6 GC molecules per sperm (resulting in a total GC concentration of 0.25 µM), a value of $10^7\ M^{-1}s^{-1}$ for k_{on}, and a value of $10^{-2}\ s^{-1}$ for k_{off}.

Single-cell measurements

Motility was studied in observation chambers with a depth of 100 µm using an inverted microscope (IX71; Olympus) equipped with a 20× objective (NA 0.75; U Plan S Apochromat; Olympus). Photolysis of caged compounds was achieved using a mercury lamp (U-RFL-T; Olympus). The light was passed through a band pass filter (H350/50; Semrock), and the irradiation time (25 ms) was controlled by a mechanical shutter (VS25; Uniblitz Vincent Associates). Laser stroboscopic illumination (2-ms pulse at 488-nm wavelength) was generated using an Argon/Krypton laser (Innova 70C; Coherent, Inc.) and an acousto-optical tunable filter (AA Opto-Electronic Company). The fluorescence was passed through a 500-nm long pass filter (Omega Optical, Inc.). Images where collected at 150 frames/s using an EM charge-coupled device (CCD) camera (DU-897D; Andor Technology). We used custom-made postacquisition programs written in MATLAB (MathWorks) to track swimming sperm and to measure time-resolved changes in fluorescence. We used a second order Savitzky–Golay filter to extract the averaged path from tracking of the sperm head.

Published September 17, 2012

Numerical reconstruction of the swimming path

To reconstruct the average swimming path from changes in fluorescence ($\Delta F/F_0$) obtained with the stopped-flow apparatus, we made use of the linear relationship between the curvature of the swimming path $\kappa(t)$ and the time derivative of the Ca^{2+} signal:

$$\kappa(t) = \kappa_1 + \beta \frac{d(\Delta F/F_0)}{dt}, \quad (4)$$

wherein κ_1 is the basal curvature after stimulation, and β is a rescaling factor (Alvarez et al., 2012). Because the amplitude of the Ca^{2+} signals obtained with the stopped-flow apparatus and single-cell recordings differ, Ca^{2+} signals were renormalized. Typically, saturating stimulation by cGMP release induced a maximal $\Delta F/F_0$ of ∼50% using the stopped-flow device, whereas single-cell measurements gave a maximal $\Delta F/F_0$ of ∼400% (Fig. 5 A in Alvarez et al., 2012). The difference in $\Delta F/F_0$ is probably caused by the lower value of the basal fluorescence (F_0) obtained in the microscope owing to the background subtraction performed on the images. The renormalized Ca^{2+} signal was converted to curvature $\kappa(t)$ using Eq. 4. Finally, the trajectory was numerically calculated by integration of the 2D Frenet–Serret equations using $\kappa(t)$ and a constant swimming speed of 150 µm/s.

Determination of resact content of eggs

10 µl of released eggs were suspended in 10-ml ASW and incubated for 60 min; the cell suspension was kept homogenous by occasional inversion of the Falcon tube. Eggs in a 5-µl suspension were counted under the microscope. At the end of the incubation and after sedimentation of eggs, 5–10-µl aliquots were taken and appropriately diluted to adjust the resact concentration in the picomolar range. The resact concentration was determined by mixing the diluted samples in the stopped-flow device with Fluo-4–loaded sperm and calibrating the resact-induced Ca^{2+} signals with known resact standards (as in Fig. S1, C and D). The concentration per egg was calculated assuming an egg radius of 50 µm. The radius in the literature varies between 37.5 and 75 µm depending on shape, age, and whether eggs are fully hydrated or not (Harvey, 1932; Goldforb et al., 1935; Bolton et al., 2000).

Preparation of Alexa Fluor 488–resact

The linear peptide was synthesized automatically with a peptide synthesizer (ABI 433A; Invitrogen) by the solid-phase method using standard *N*-(9-fluorenyl)methoxycarbonyl chemistry (Coin et al., 2007) in a batch mode on polyethylene glycol resins (0.2 mmol/g; standard rink amide; Rapp Polymere). After final cleavage and deprotection with TFA/H_2O/tri-isopropylsilane (8.5:1:0.5) for 3 h at room temperature, the peptide was precipitated with cold diethyl ether. For the formation of the intramolecular disulfide, 1 mg/ml linear peptide was air oxidized in bicarbonate buffer, pH 8.5, for 16 h at room temperature. Crude resact was purified by preparative reversed-phase HPLC (C-18) using acetonitrile gradient in aqueous 0.1% TFA. To introduce Alexa Fluor 488 carboxylic acid, the corresponding succinimidyl ester (mixed isomers; 5 mg and 7 µmol; Molecular Probes) dissolved in 100 µl dimethylformamide was added to 7 µmol resact. 50 µl bicarbonate (0.1 M) buffer, pH 8.5, was added to the clear solution, and the reaction was followed by analytical HPLC using fluorescence detection. After 2 h, Alexa Fluor 488–resact was isolated by preparative HPLC and characterized by electrospray ionization mass spectrometry (M_{calc} = 1,758.6; $[M+H]_{exp}$ = 1,760.36), in which M_{calc} is the calculated monoisotopic molecular mass of the product, and $[M+H]_{exp}$ was calculated from [(m/z)+H] peaks found for z = 3 with 587.4533 and z = 2 with 880.66.

Dual-focus fluorescence correlation spectroscopy

The dual-focus fluorescence correlation spectroscopy measurements were performed as previously described in Dertinger et al. (2007). In summary, the light from two identical, linearly polarized pulsed diode lasers (wavelength of 485 nm and pulse duration of 50-ps full width at half-maximum) was combined by a polarizing beam splitter. Both lasers were pulsed alternately with a repetition rate of 40 MHz. The average power of the lasers was 3 µW each. Both beams were coupled into a polarization-maintaining single-mode fiber. At the fiber output, the light was collimated and reflected by a dichroic mirror (FITC/TRITC; Chroma Technology Corp.) toward the microscope's objective (U Plan S Apochromat 60× water, 1.2 NA; Olympus). Before entering the objective, the light was passed through a Nomarski prism, deflecting the light from both laser diodes into slightly different directions, so that, after focusing, two laterally shifted but overlapping excitation foci were obtained with an ∼420-nm distance.

Fluorescence was collected by the same objective, passed through the dichroic mirror, and focused onto a single circular aperture (diameter of 150 µm). After the pinhole, the light was collimated, split by a 50/50 beam splitter, and focused onto two single-photon avalanche diodes (SPCM-AQR-13; PerkinElmer). Single-photon counting electronics (HydraHarp 400; PicoQuant GmbH) recorded the signals of both detectors independently with an absolute temporal resolution of 2 ps on a common time frame.

Recording photon detection times with picosecond resolution allows associating each fluorescence photon with the exciting laser pulse and thus with the respective focus. With this information, the auto- and cross correlation curves were calculated. Finally, a global fit of the data was made with a model using three fit parameters: two parameters for the molecule detection function and the diffusion coefficient.

Measurements of resact labeled with Alexa Fluor 488 (Invitrogen) were performed at 22°C in ASW. The diffusion constant of the labeled peptide (molecular weight [MW] = 1,772.3 g/mol) under these conditions was 231 ± 7 µm²/s (nine experiments). The value for free resact (molecular weight = 1,246.5 g/mol) in ASW at 16°C can be extrapolated using the temperature dependence of the viscosity of sea water (ή (22°C) = 1.025 mPa s; ή (16°C) = 1.183 mPa s; El-Dessouky and Ettouney, 2002) and the mass dependence of the radius *r* of a Gaussian chain-type polymer

$$r_1 / r_2 = \sqrt{\frac{MW_1}{MW_2}}$$

Rubinstein and Colby, 2003). Using these parameters, the extrapolated diffusion constant of resact (D_{resact}) in ASW at 16°C is 239 ± 7 µm²/s. Using either value does not significantly alter the gradient simulations.

Simulation of resact gradient

The concentration profiles of resact were computed by solving the diffusion equation using COMSOL (COMSOL Multiphysics GmbH). A semispherical geometry (radius of 10 cm) was simulated using an axial symmetric pseudo-3D finite element model. Time-dependent concentration profiles were computed for different synthesis rates over a time span of 60 min. The mesh of the finite element model was refined until relative changes in the obtained concentration profiles were $<10^{-9}$.

Minimal gradient calculations

To determine the rate of resact molecules absorbed by sperm, we consider the flagellum as a rod-shaped structure with a length of l_f = 50 µm and a diameter of d_f = 0.3 µm. The maximal absorption rate *k* can be calculated from the flux of molecules onto ellipsoid, flagella-like objects is

$$k = \frac{4\pi a N_A}{\ln(2a/b)} D$$

(Berg, 1993), wherein *D* is the diffusion constant of the molecule (D_{Resact} = 239 ± 7 µm²/s), *a* and *b* are the long and short semiaxes, respectively, of an ellipsoid of revolution, and N_A is Avogadro's number. For the flagellum, we use $a = l_f/2$ = 25 µm and $b = d_f/2$ = 0.15 µm. The number of molecules absorbed at concentration *c* within time *t* is $N_{abs} = kct$, with a Poisson standard deviation $\sigma(N_{abs}) = \sqrt{N_{abs}}$. For a period *T* of circular swimming ($T = 2\pi r/s$), the number of observed molecules is $N_{abs} = 2\pi rkc/s$, wherein *r* is the radius of circular swimming and *s* is the swimming speed. For N_{abs} = 1, i.e., the minimal number of molecules absorbed during one period, the minimal concentration becomes c_{min} = 44 fM.

To determine the minimal gradient that supports chemotaxis, the gradient is considered to be approximately linear. Using a local coordinate system with the *x′* axis pointing toward the egg (Fig. 8 D), the concentration can be described by $c(x') = g\,x' + c_{mean}$, wherein *g* is the gradient dc/dx, and c_{mean} is the concentration at the center of the circle. For boundaries $c(x' = -r) = c_1$ and $c(x' = r) = c_2$ (Fig. 8 B), $g = (c_2 - c_1)/2r$ and $c_{mean} = (c_2 + c_1)/2$. Thus, for any point in time, the concentration along the circular path is given by $c(t) = g\,r\sin(2\pi\,t/T) + c_{mean}$. The integral over both semicircles (t_1 = 0 to $T/2$ and $t_2 = T/2$ to *T*) yields the difference $\Delta N_{abs} = 4g\,r^2\,k/s$. As criterion for successful chemotaxis, we define that ΔN_{abs} must be equal or larger than the noise $\sqrt{N_{abs}}$ because of statistical fluctuations, i.e., the *S/N* ratio is ≥1. Therefore, the minimal detectable gradient becomes

$$g_{\min} = \sqrt{\frac{\pi s c}{8 k r^3}}.$$

Chemotaxis occurs in regions where $g \geq g_{min}$.

Published September 17, 2012

The minimal gradient g_{min} scales with $\sqrt{s / r^3}$. Upon stimulation with cGMP, the swimming speed s increased from 135 ± 17 µm/s to 180 ± 20 µm/s (n = 23). Moreover, sperm increase their mean swimming radius from ~26 to 83 µm. This increase can be considered as a mechanism to enhance the sensitivity of gradient sensing. In fact, g_{min} required after stimulation is five times smaller than that before stimulation. In addition, g_{min} is a function of the ambient concentration c; larger values of c demand also steeper gradients for successful chemotaxis.

Statistics

All values are means ± SD (number of experiments).

Online supplemental material

Fig. S1 shows the scheme of the sampling and resetting experiments using caged resact and the temporal accuracy of paired stimuli and explains the assay used for the calibration of resact released from the caged precursor by a flash of light. Fig. S2 shows a complete time course of the Ca^{2+} signals obtained from sampling and resetting experiments. Fig. S3 shows the pitfalls and unspecific effects of a commonly used Na^+/Ca^{2+} exchanger blocker (KB-R7943 mesylate) in studying Ca^{2+} homeostasis in sea urchin sperm. Table S1, S2, and S3 list the peptides identified by mass spectrometry analysis of sperm flagella proteome—Na^+/Ca^{2+} exchanger from *A. punctulata* (Table S1), Na^+/Ca^{2+} exchanger from *S. purpuratus* (Table S2), and Ca^{2+} ATPase from *S. purpuratus* (Table S3). Video 1 shows resetting of Ca^{2+} signals in single moving sperm. Online supplemental material is available at http://www.jcb.org/cgi/content/full/jcb.201204024/DC1.

We thank Drs. Timo Strünker and Dagmar Wachten for helpful discussions and critically reading the manuscript. We thank Dr. Victor Sourjik (Heidelberg) for helpful discussions on bacterial chemotaxis. We thank Heike Krause for preparing the manuscript. The caged compounds were kindly provided by Dr. Volker Hagen.

This work was supported by the German Research Foundation and the Fonds der Chemischen Industrie.

Author contributions: N.D. Kashikar and U.B. Kaupp conceived the project and designed the experiments. N.D. Kashikar, L. Alvarez, and I. Gregor further developed the stopped-flow and photolysis set-up. N.D. Kashikar, L. Alvarez, I. Gregor, O. Jäckle, and U.B. Kaupp performed the experiments. N.D. Kashikar, I. Gregor, R. Seifert, O. Jäckle, and L. Alvarez analyzed the data. I. Gregor and L. Alvarez designed the model for minimal gradient detection. M. Beyermann synthesized Alexa Fluor 488–resact. E. Krause performed mass spectrometry experiments. N.D. Kashikar, L. Alvarez, R. Seifert, I. Gregor, and U.B. Kaupp wrote the manuscript. All authors commented on and edited the text.

Submitted: 5 April 2012
Accepted: 16 August 2012

References

Alvarez, L., L. Dai, B.M. Friedrich, N.D. Kashikar, I. Gregor, R. Pascal, and U.B. Kaupp. 2012. The rate of change in Ca^{2+} concentration controls sperm chemotaxis. *J. Cell Biol.* 196:653–663. http://dx.doi.org/10.1083/jcb.201106096

Babcock, D.F., M.M. Bosma, D.E. Battaglia, and A. Darszon. 1992. Early persistent activation of sperm K^+ channels by the egg peptide speract. *Proc. Natl. Acad. Sci. USA*. 89:6001–6005. http://dx.doi.org/10.1073/pnas.89.13.6001

Berg, H.C. 1993. Random Walks in Biology. Princeton University Press, Princeton, NJ. 152 pp.

Berg, H.C., and E.M. Purcell. 1977. Physics of chemoreception. *Biophys. J.* 20:193–219. http://dx.doi.org/10.1016/S0006-3495(77)85544-6

Blaustein, M.P., and W.J. Lederer. 1999. Sodium/calcium exchange: its physiological implications. *Physiol. Rev.* 79:763–854.

Böhmer, M., Q. Van, I. Weyand, V. Hagen, M. Beyermann, M. Matsumoto, M. Hoshi, E. Hildebrand, and U.B. Kaupp. 2005. Ca^{2+} spikes in the flagellum control chemotactic behavior of sperm. *EMBO J.* 24:2741–2752. http://dx.doi.org/10.1038/sj.emboj.7600744

Bolton, T.F., F.I.M. Thomas, and C.N. Leonard. 2000. Maternal energy investment in eggs and jelly coats surrounding eggs of the echinoid *Arbacia punctulata*. *Biol. Bull.* 199:1–5. http://dx.doi.org/10.2307/1542700

Bönigk, W., A. Loogen, R. Seifert, N. Kashikar, C. Klemm, E. Krause, V. Hagen, E. Kremmer, T. Strünker, and U.B. Kaupp. 2009. An atypical CNG channel activated by a single cGMP molecule controls sperm chemotaxis. *Sci. Signal.* 2:ra68. http://dx.doi.org/10.1126/scisignal.2000516

Brokaw, C.J. 1959. Random and oriented movements of bracken spermatozoids. *J. Cell. Comp. Physiol.* 54:95–101. http://dx.doi.org/10.1002/jcp.1030540110

Burnett, L.A., D.M. Anderson, A. Rawls, A.L. Bieber, and D.E. Chandler. 2011. Mouse sperm exhibit chemotaxis to allurin, a truncated member of the cysteine-rich secretory protein family. *Dev. Biol.* 360:318–328. http://dx.doi.org/10.1016/j.ydbio.2011.09.028

Burns, M.E., and D.A. Baylor. 2001. Activation, deactivation, and adaptation in vertebrate photoreceptor cells. *Annu. Rev. Neurosci.* 24:779–805. http://dx.doi.org/10.1146/annurev.neuro.24.1.779

Cervetto, L., L. Lagnado, R.J. Perry, D.W. Robinson, and P.A. McNaughton. 1989. Extrusion of calcium from rod outer segments is driven by both sodium and potassium gradients. *Nature*. 337:740–743. http://dx.doi.org/10.1038/337740a0

Coin, I., M. Beyermann, and M. Bienert. 2007. Solid-phase peptide synthesis: from standard procedures to the synthesis of difficult sequences. *Nat. Protoc.* 2:3247–3256. http://dx.doi.org/10.1038/nprot.2007.454

Corkidi, G., B. Taboada, C.D. Wood, A. Guerrero, and A. Darszon. 2008. Tracking sperm in three-dimensions. *Biochem. Biophys. Res. Commun.* 373:125–129. http://dx.doi.org/10.1016/j.bbrc.2008.05.189

Crenshaw, H.C., and L. Edelstein-Keshet. 1993. Orientation by helical motion - II. Changing the direction of the axis of motion. *Bull. Math. Biol.* 55: 213–230.

Dertinger, T., V. Pacheco, I. von der Hocht, R. Hartmann, I. Gregor, and J. Enderlein. 2007. Two-focus fluorescence correlation spectroscopy: a new tool for accurate and absolute diffusion measurements. *ChemPhysChem*. 8:433–443. http://dx.doi.org/10.1002/cphc.200600638

Dertinger, T., A. Loman, B. Ewers, C.B. Müller, B. Krämer, and J. Enderlein. 2008. The optics and performance of dual-focus fluorescence correlation spectroscopy. *Opt. Express*. 16:14353–14368. http://dx.doi.org/10.1364/OE.16.014353

Dusenbery, D.B. 2009. Living at Micro Scale: The Unexpected Physics of Being Small. Harvard University Press, Cambridge, MA. 416 pp.

Eatock, R.A., D.P. Corey, and A.J. Hudspeth. 1987. Adaptation of mechanoelectrical transduction in hair cells of the bullfrog's sacculus. *J. Neurosci.* 7: 2821–2836.

Eisenbach, M., and L.C. Giojalas. 2006. Sperm guidance in mammals - an unpaved road to the egg. *Nat. Rev. Mol. Cell Biol.* 7:276–285. http://dx.doi.org/10.1038/nrm1893

El-Dessouky, H.T., and H.M. Ettouney. 2002. Fundamentals of Salt Water Desalination. Elsevier Science, Amsterdam/New York. 670 pp.

Friedrich, B.M., and F. Jülicher. 2007. Chemotaxis of sperm cells. *Proc. Natl. Acad. Sci. USA*. 104:13256–13261. http://dx.doi.org/10.1073/pnas.0703530104

Gakamsky, A., L. Armon, and M. Eisenbach. 2009. Behavioral response of human spermatozoa to a concentration jump of chemoattractants or intracellular cyclic nucleotides. *Hum. Reprod.* 24:1152–1163. http://dx.doi.org/10.1093/humrep/den409

Galindo, B.E., J.L. de la Vega-Beltrán, P. Labarca, V.D. Vacquier, and A. Darszon. 2007. Sp-tetraKCNG: A novel cyclic nucleotide gated K^+ channel. *Biochem. Biophys. Res. Commun.* 354:668–675. http://dx.doi.org/10.1016/j.bbrc.2007.01.035

Goldforb, A.J., V. Schechter, and M. Landowne. 1935. Change in size and shape of ageing eggs (*Arbacia punctulata*). *Biol. Bull.* 68:180–190. http://dx.doi.org/10.2307/1537262

Guerrero, A., T. Nishigaki, J. Carneiro, Yoshiro Tatsu, C.D. Wood, and A. Darszon. 2010a. Tuning sperm chemotaxis by calcium burst timing. *Dev. Biol.* 344:52–65. http://dx.doi.org/10.1016/j.ydbio.2010.04.013

Guerrero, A., C.D. Wood, T. Nishigaki, J. Carneiro, and A. Darszon. 2010b. Tuning sperm chemotaxis. *Biochem. Soc. Trans.* 38:1270–1274. http://dx.doi.org/10.1042/BST0381270

Guerrero, A., J. Carneiro, A. Pimentel, C.D. Wood, G. Corkidi, and A. Darszon. 2011. Strategies for locating the female gamete: the importance of measuring sperm trajectories in three spatial dimensions. *Mol. Hum. Reprod.* 17:511–523. http://dx.doi.org/10.1093/molehr/gar042

Gunaratne, H.J., and V.D. Vacquier. 2006. Evidence for a secretory pathway Ca^{2+}-ATPase in sea urchin spermatozoa. *FEBS Lett.* 580:3900–3904. http://dx.doi.org/10.1016/j.febslet.2006.06.019

Hackos, D.H., and J.I. Korenbrot. 1997. Calcium modulation of ligand affinity in the cyclic GMP-gated ion channels of cone photoreceptors. *J. Gen. Physiol.* 110:515–528. http://dx.doi.org/10.1085/jgp.110.5.515

Hagen, V., J. Bendig, S. Frings, T. Eckardt, S. Helm, D. Reuter, and U.B. Kaupp. 2001. Highly efficient and ultrafast phototriggers for cAMP and cGMP by using long-wavelength UV/Vis-activation. *Angew. Chem. Int. Ed. Engl.* 40:1045–1048. http://dx.doi.org/10.1002/1521-3773(20010316)40:6<1045::AID-ANIE10450>3.0.CO;2-F

Hagen, V., S. Frings, J. Bendig, D. Lorenz, B. Wiesner, and U.B. Kaupp. 2002. Fluorescence spectroscopic quantification of the release of cyclic nucleotides from photocleavable [bis(carboxymethoxy)coumarin-4-yl] methyl esters inside cells. *Angew. Chem. Int. Ed. Engl.* 41:3625–3628: 3516. http://dx.doi.org/10.1002/1521-3773(20021004)41:19<3625::AID-ANIE3625>3.0.CO;2-J

Hagen, V., S. Frings, B. Wiesner, S. Helm, U.B. Kaupp, and J. Bendig. 2003. [7-(Dialkylamino)coumarin-4-yl]methyl-caged compounds as ultrafast and effective long-wavelength phototriggers of 8-bromo-substituted cyclic nucleotides. *ChemBioChem.* 4:434–442. http://dx.doi.org/10.1002/cbic.200300561

Harvey, E.B. 1954. Electrical method of determining the sex of sea urchins. *Nature*. 173:86. http://dx.doi.org/10.1038/173086a0

Harvey, E.N. 1932. Physical and chemical constants of the egg of the sea urchin, *Arbacia punctulata. Biol. Bull.* 62:141–154. http://dx.doi.org/10.2307/1537546

Hille, B. 2001. Ionic Channels of Excitable Membranes. Third edition. Sinauer Associates, Sunderland, MA. 814 pp.

Iglesias, P.A. 2012. A systems biology view of adaptation in sensory mechanisms. *Adv. Exp. Med. Biol.* 736:499–516. http://dx.doi.org/10.1007/978-1-4419-7210-1_29

Jékely, G. 2009. Evolution of phototaxis. *Philos. Trans. R. Soc. Lond. B Biol. Sci.* 364:2795–2808. http://dx.doi.org/10.1098/rstb.2009.0072

Jékely, G., J. Colombelli, H. Hausen, K. Guy, E. Stelzer, F. Nédélec, and D. Arendt. 2008. Mechanism of phototaxis in marine zooplankton. *Nature*. 456:395–399. http://dx.doi.org/10.1038/nature07590

Kalinin, Y.V., L. Jiang, Y. Tu, and M. Wu. 2009. Logarithmic sensing in *Escherichia coli* bacterial chemotaxis. *Biophys. J.* 96:2439–2448. http://dx.doi.org/10.1016/j.bpj.2008.10.027

Kaupp, U.B., J. Solzin, E. Hildebrand, J.E. Brown, A. Helbig, V. Hagen, M. Beyermann, F. Pampaloni, and I. Weyand. 2003. The signal flow and motor response controlling chemotaxis of sea urchin sperm. *Nat. Cell Biol.* 5:109–117. http://dx.doi.org/10.1038/ncb915

Kaupp, U.B., N.D. Kashikar, and I. Weyand. 2008. Mechanisms of sperm chemotaxis. *Annu. Rev. Physiol.* 70:93–117. http://dx.doi.org/10.1146/annurev.physiol.70.113006.100654

Kilic, F., N.D. Kashikar, R. Schmidt, L. Alvarez, L. Dai, I. Weyand, B. Wiesner, N. Goodwin, V. Hagen, and U.B. Kaupp. 2009. Caged progesterone: a new tool for studying rapid nongenomic actions of progesterone. *J. Am. Chem. Soc.* 131:4027–4030. http://dx.doi.org/10.1021/ja808334f

Kleene, S.J. 2008. The electrochemical basis of odor transduction in vertebrate olfactory cilia. *Chem. Senses*. 33:839–859. http://dx.doi.org/10.1093/chemse/bjn048

Koch, K.-W., and L. Stryer. 1988. Highly cooperative feedback control of retinal rod guanylate cyclase by calcium ions. *Nature*. 334:64–66. http://dx.doi.org/10.1038/334064a0

Kurahashi, T., and A. Menini. 1997. Mechanism of odorant adaptation in the olfactory receptor cell. *Nature*. 385:725–729. http://dx.doi.org/10.1038/385725a0

Lagnado, L., and P.A. McNaughton. 1990. Electrogenic properties of the Na:Ca exchange. *J. Membr. Biol.* 113:177–191. http://dx.doi.org/10.1007/BF01870070

Lagnado, L., L. Cervetto, and P.A. McNaughton. 1988. Ion transport by the Na-Ca exchange in isolated rod outer segments. *Proc. Natl. Acad. Sci. USA*. 85:4548–4552. http://dx.doi.org/10.1073/pnas.85.12.4548

Lange, S., M. Sylvester, M. Schümann, C. Freund, and E. Krause. 2010. Identification of phosphorylation-dependent interaction partners of the adapter protein ADAP using quantitative mass spectrometry: SILAC vs (18)O-labeling. *J. Proteome Res.* 9:4113–4122. http://dx.doi.org/10.1021/pr1003054

Laughlin, S.B. 1989. The role of sensory adaptation in the retina. *J. Exp. Biol.* 146:39–62.

Lazier, J.R.N., and K.H. Mann. 1989. Turbulence and the diffusive layers around small organisms. *Deep-Sea Res.* 36:1721–1733. http://dx.doi.org/10.1016/0198-0149(89)90068-X

Lillie, F.R. 1912. The production of sperm iso-agglutinins by ova. *Science*. 36:527–530. http://dx.doi.org/10.1126/science.36.929.527

Lillie, F.R. 1913. The mechanism of fertilization. *Science*. 38:524–528. http://dx.doi.org/10.1126/science.38.980.524

Lishko, P.V., Y. Kirichok, D. Ren, B. Navarro, J.J. Chung, and D.E. Clapham. 2012. The control of male fertility by spermatozoan ion channels. *Annu. Rev. Physiol.* 74:453–475. http://dx.doi.org/10.1146/annurev-physiol-020911-153258

Lockery, S.R. 2011. The computational worm: spatial orientation and its neuronal basis in *C. elegans. Curr. Opin. Neurobiol.* 21:782–790. http://dx.doi.org/10.1016/j.conb.2011.06.009

Macnab, R.M., and D.E. Koshland Jr. 1972. The gradient-sensing mechanism in bacterial chemotaxis. *Proc. Natl. Acad. Sci. USA*. 69:2509–2512. http://dx.doi.org/10.1073/pnas.69.9.2509

Mao, H., P.S. Cremer, and M.D. Manson. 2003. A sensitive, versatile microfluidic assay for bacterial chemotaxis. *Proc. Natl. Acad. Sci. USA*. 100: 5449–5454. http://dx.doi.org/10.1073/pnas.0931258100

Matsumoto, M., J. Solzin, A. Helbig, V. Hagen, S.-I. Ueno, O. Kawase, Y. Maruyama, M. Ogiso, M. Godde, H. Minakata, et al. 2003. A sperm-activating peptide controls a cGMP-signaling pathway in starfish sperm. *Dev. Biol.* 260:314–324. http://dx.doi.org/10.1016/S0012-1606(03)00236-7

Matthews, H.R., G.L. Fain, R.L. Murphy, and T.D. Lamb. 1990. Light adaptation in cone photoreceptors of the salamander: a role for cytoplasmic calcium. *J. Physiol.* 420:447–469.

Mengerink, K.J., and V.D. Vacquier. 2004. Isolation of sea urchin sperm plasma membranes. *Methods Mol. Biol.* 253:141–150.

Mesibov, R., G.W. Ordal, and J. Adler. 1973. The range of attractant concentrations for bacterial chemotaxis and the threshold and size of response over this range. Weber law and related phenomena. *J. Gen. Physiol.* 62: 203–223. http://dx.doi.org/10.1085/jgp.62.2.203

Morita, M., M. Kitamura, A. Nakajima, E. Sri Susilo, A. Takemura, and M. Okuno. 2009. Regulation of sperm flagellar motility activation and chemotaxis caused by egg-derived substance(s) in sea cucumber. *Cell Motil. Cytoskeleton*. 66:202–214. http://dx.doi.org/10.1002/cm.20343

Neumann, S., C.H. Hansen, N.S. Wingreen, and V. Sourjik. 2010. Differences in signalling by directly and indirectly binding ligands in bacterial chemotaxis. *EMBO J.* 29:3484–3495. http://dx.doi.org/10.1038/emboj.2010.224

Nishigaki, T., C.D. Wood, Y. Tatsu, N. Yumoto, T. Furuta, D. Elias, K. Shiba, S.A. Baba, and A. Darszon. 2004. A sea urchin egg jelly peptide induces a cGMP-mediated decrease in sperm intracellular Ca^{2+} before its increase. *Dev. Biol.* 272:376–388. http://dx.doi.org/10.1016/j.ydbio.2004.04.035

Olson, J.H., X. Xiang, T. Ziegert, A. Kittelson, A. Rawls, A.L. Bieber, and D.E. Chandler. 2001. Allurin, a 21-kDa sperm chemoattractant from *Xenopus* egg jelly, is related to mammalian sperm-binding proteins. *Proc. Natl. Acad. Sci. USA*. 98:11205–11210. http://dx.doi.org/10.1073/pnas.211316798

Palmer, L. 1937. The shedding reaction in *Arbacia punctulata. Physiol. Zool.* 10:352–367.

Peng, A.W., F.T. Salles, B. Pan, and A.J. Ricci. 2011. Integrating the biophysical and molecular mechanisms of auditory hair cell mechanotransduction. *Nat Commun*. 2:523. http://dx.doi.org/10.1038/ncomms1533

Perez-Reyes, E. 2003. Molecular physiology of low-voltage-activated t-type calcium channels. *Physiol. Rev.* 83:117–161.

Publicover, S., C.V. Harper, and C. Barratt. 2007. $[Ca^{2+}]_i$ signalling in sperm—making the most of what you've got. *Nat. Cell Biol.* 9:235–242. http://dx.doi.org/10.1038/ncb0307-235

Pugh, E.N., Jr., and T.D. Lamb. 2000. Phototransduction in vertebrate rods and cones: Molecular mechanisms of amplification, recovery and light adaptation. *In* Handbook of Biological Physics. Vol. 3. D.G. Stavenga, W.J. de Grip, and E.N. Pugh Jr., editors. Elsevier Science, Amsterdam. 183–255.

Pugh, E.N., Jr., S. Nikonov, and T.D. Lamb. 1999. Molecular mechanisms of vertebrate photoreceptor light adaptation. *Curr. Opin. Neurobiol.* 9: 410–418. http://dx.doi.org/10.1016/S0959-4388(99)80062-2

Rebrik, T.I., and J.I. Korenbrot. 2004. In intact mammalian photoreceptors, Ca^{2+}-dependent modulation of cGMP-gated ion channels is detectable in cones but not in rods. *J. Gen. Physiol.* 123:63–75. http://dx.doi.org/10.1085/jgp.200308952

Rebrik, T.I., I. Botchkina, V.Y. Arshavsky, C.M. Craft, and J.I. Korenbrot. 2012. CNG-modulin: a novel Ca-dependent modulator of ligand sensitivity in cone photoreceptor cGMP-gated ion channels. *J. Neurosci.* 32: 3142–3153. http://dx.doi.org/10.1523/JNEUROSCI.5518-11.2012

Riffell, J.A., and R.K. Zimmer. 2007. Sex and flow: the consequences of fluid shear for sperm-egg interactions. *J. Exp. Biol.* 210:3644–3660. http://dx.doi.org/10.1242/jeb.008516

Riffell, J.A., P.J. Krug, and R.K. Zimmer. 2002. Fertilization in the sea: the chemical identity of an abalone sperm attractant. *J. Exp. Biol.* 205: 1439–1450.

Rubinstein, M., and R.H. Colby. 2003. Polymer Physics. Oxford University Press, New York. 512 pp.

Shiba, K., S.A. Baba, T. Inoue, and M. Yoshida. 2008. Ca^{2+} bursts occur around a local minimal concentration of attractant and trigger sperm chemotactic response. *Proc. Natl. Acad. Sci. USA*. 105:19312–19317. http://dx.doi.org/10.1073/pnas.0808580105

Shimomura, H., L.J. Dangott, and D.L. Garbers. 1986. Covalent coupling of a resact analogue to guanylate cyclase. *J. Biol. Chem.* 261:15778–15782.

Sourjik, V., and J.P. Armitage. 2010. Spatial organization in bacterial chemotaxis. *EMBO J.* 29:2724–2733. http://dx.doi.org/10.1038/emboj.2010.178

Strünker, T., I. Weyand, W. Bönigk, Q. Van, A. Loogen, J.E. Brown, N. Kashikar, V. Hagen, E. Krause, and U.B. Kaupp. 2006. A K^+-selective cGMP-gated ion channel controls chemosensation of sperm. *Nat. Cell Biol.* 8: 1149–1154. http://dx.doi.org/10.1038/ncb1473

Su, Y.H., and V.D. Vacquier. 2002. A flagellar K^+-dependent Na^+/Ca^{2+} exchanger keeps Ca^{2+} low in sea urchin spermatozoa. *Proc. Natl. Acad. Sci. USA*. 99: 6743–6748. http://dx.doi.org/10.1073/pnas.102186699

Swaney, K.F., C.H. Huang, and P.N. Devreotes. 2010. Eukaryotic chemotaxis: a network of signaling pathways controls motility, directional sensing, and polarity. *Annu Rev Biophys*. 39:265–289. http://dx.doi.org/10.1146/annurev.biophys.093008.131228

Thar, R., and T. Fenchel. 2001. True chemotaxis in oxygen gradients of the sulfur-oxidizing bacterium *Thiovulum majus*. *Appl. Environ. Microbiol.* 67:3299–3303. http://dx.doi.org/10.1128/AEM.67.7.3299-3303.2001

Torre, V., J.F. Ashmore, T.D. Lamb, and A. Menini. 1995. Transduction and adaptation in sensory receptor cells. *J. Neurosci.* 15:7757–7768.

Vacquier, V.D., and G.W. Moy. 1986. Stoichiometry of phosphate loss from sea urchin sperm guanylate cyclase during fertilization. *Biochem. Biophys. Res. Commun.* 137:1148–1152. http://dx.doi.org/10.1016/0006-291X(86)90345-1

Vladimirov, N., and V. Sourjik. 2009. Chemotaxis: how bacteria use memory. *Biol. Chem.* 390:1097–1104. http://dx.doi.org/10.1515/BC.2009.130

Wang, C.J., A. Bergmann, B. Lin, K. Kim, and A. Levchenko. 2012. Diverse sensitivity thresholds in dynamic signaling responses by social amoebae. *Sci. Signal.* 5:ra17. http://dx.doi.org/10.1126/scisignal.2002449

Ward, G.E., and V.D. Vacquier. 1983. Dephosphorylation of a major sperm membrane protein is induced by egg jelly during sea urchin fertilization. *Proc. Natl. Acad. Sci. USA*. 80:5578–5582. http://dx.doi.org/10.1073/pnas.80.18.5578

Ward, G.E., C.J. Brokaw, D.L. Garbers, and V.D. Vacquier. 1985. Chemotaxis of *Arbacia punctulata* spermatozoa to resact, a peptide from the egg jelly layer. *J. Cell Biol.* 101:2324–2329. http://dx.doi.org/10.1083/jcb.101.6.2324

Wood, C.D., T. Nishigaki, T. Furuta, S.A. Baba, and A. Darszon. 2005. Real-time analysis of the role of Ca^{2+} in flagellar movement and motility in single sea urchin sperm. *J. Cell Biol.* 169:725–731. http://dx.doi.org/10.1083/jcb.200411001

Yoshida, M., and K. Yoshida. 2011. Sperm chemotaxis and regulation of flagellar movement by Ca^{2+}. *Mol. Hum. Reprod.* 17:457–465. http://dx.doi.org/10.1093/molehr/gar041

Yoshida, M., M. Murata, K. Inaba, and M. Morisawa. 2002. A chemoattractant for ascidian spermatozoa is a sulfated steroid. *Proc. Natl. Acad. Sci. USA*. 99:14831–14836. http://dx.doi.org/10.1073/pnas.242470599

Zimmer, R.K., and J.A. Riffell. 2011. Sperm chemotaxis, fluid shear, and the evolution of sexual reproduction. *Proc. Natl. Acad. Sci. USA*. 108:13200–13205. http://dx.doi.org/10.1073/pnas.1018666108